Calhoun
Institutional Archive of the Naval Postgraduate School

Calhoun: The NPS Institutional Archive

DSpace Repository

Theses and Dissertations 1. Thesis and Dissertation Collection, all items

1995-03

Plasma formation on the anode of the Flash X-ray facility

Stamatopoulos, Vassillios

Monterey, California. Naval Postgraduate School

http://hdl.handle.net/10945/7549

This publication is a work of the U.S. Government as defined in Title 17, United States Code, Section 101. Copyright protection is not available for this work in the United States.

Downloaded from NPS Archive: Calhoun

DUDLEY
KNOX
LIBRARY

Calhoun is the Naval Postgraduate School's public access digital repository for research materials and institutional publications created by the NPS community. Calhoun is named for Professor of Mathematics Guy K. Calhoun, NPS's first appointed -- and published -- scholarly author.

Dudley Knox Library / Naval Postgraduate School
411 Dyer Road / 1 University Circle
Monterey, California USA 93943

http://www.nps.edu/library

NAVAL POSTGRADUATE SCHOOL
Monterey, California

THESIS

PLASMA FORMATION ON THE ANODE OF THE FLASH X-RAY FACILITY

by

Vassilios Stamatopoulos

March, 1995

Thesis Advisor: F. Schwirzke
Thesis Co-Advisors: X.K. Maruyama
R.W. Ashton

Approved for public release; distribution is unlimited.

Thesis
S67223

DUDLEY KNOX LIBRARY
NAVAL POSTGRADUATE SCHOOL
MONTEREY CA 93943-5101

REPORT DOCUMENTATION PAGE	Form Approved OMB No. 0704

Public reporting burden for this collection of information is estimated to average 1 hour per response, including the time for reviewing instruction, searching existing data sources, gathering and maintaining the data needed, and completing and reviewing the collection of information. Send comments regarding this burden estimate or any other aspect of this collection of information, including suggestions for reducing this burden, to Washington headquarters Services, Directorate for Information Operations and Reports, 1215 Jefferson Davis Highway, Suite 1204, Arlington, VA 22202-4302, and to the Office of Management and Budget, Paperwork Reduction Project (0704-0188) Washington DC 20503.

1. AGENCY USE ONLY *(Leave blank)*	2. REPORT DATE March 1995	3. REPORT TYPE AND DATES COVERED Master's Thesis, Final

4. TITLE AND SUBTITLE PLASMA FORMATION ON THE ANODE OF THE FLASH X -RAY FACILITY	5. FUNDING NUMBERS
6. AUTHOR(S) Stamatopoulos Vassilios.	
7. PERFORMING ORGANIZATION NAME(S) AND ADDRESS(ES) Naval Postgraduate School Monterey CA 93943-5000	8. PERFORMING ORGANIZATION REPORT NUMBER
9. SPONSORING/MONITORING AGENCY NAME(S) AND ADDRESS(ES)	10. SPONSORING/MONITORING AGENCY REPORT NUMBER

11. SUPPLEMENTARY NOTES
The views expressed in this thesis are those of the author and do not reflect the official policy or position of the Department of Defense or the U.S. Government.

12a. DISTRIBUTION/AVAILABILITY STATEMENT Approved for public release; distribution unlimited	12b. DISTRIBUTION CODE

13. ABSTRACT *(maximum 200 words)* This thesis is a case of study of the mechanisms associated with the formation of plasma in a vacuum diode during the break down process. The issues brought forth in this thesis have been studied for many years but have not yet been well understood. Specifically, on the anode of a fast pulsed high vacuum diode the Explosive Electron Emission Model states that the plasma formation is caused by energy deposition on the anode electrode surface. The Desorbed Neutral Ionization model states that the neutral cloud on the anode surface contributes to the plasma formation on the anodic surface. This work presents experimental results which support the model for formation of plasma and thus spot cratering on the anode surface. The findings of our work seem to support the DNI model. However, some of the results are not predicted by the model and it is proposed that the model could be expanded into the study of the behavior of the magnetic fields during the breakdown process.

14. SUBJECT TERMS Vacuum Diode, Plasma Formation, Anode Spot, Unipolar Arc, Space Charge, Neutral Cloud.	15. NUMBER OF PAGES 110
	16. PRICE CODE

17. SECURITY CLASSIFICATION OF REPORT Unclassified	18. SECURITY CLASSIFICATION OF THIS PAGE Unclassified	19. SECURITY CLASSIFICATION OF ABSTRACT Unclassified	20. LIMITATION OF ABSTRACT UL

NSN 7540-01-280-5500

Standard Form 298 (Rev. 2-89)
Prescribed by ANSI Std. 239-18

Approved for public release; distribution is unlimited.

PLASMA FORMATION ON THE ANODE OF THE FLASH X-RAY FACILITY

by

Vassillios Stamatopoulos
Lieutenant, Junior Grade, Hellenic Navy
B.S. Hellenic Naval Academy, 1987

Submitted in partial fulfillment of the
requirements for the degree of

**MASTER OF SCIENCE IN APPLIED PHYSICS AND
MASTER OF SCIENCE IN ELECTRICAL ENGINEERING**

from the

**NAVAL POSTGRADUATE SCHOOL
March, 1995**

Author: [redacted]
Vassilios Stamatopoulos

Approved by: [redacted]
F. Schwirzke, Thesis Advisor

[redacted]
X.K. Maruyama, Thesis Co-Advisor

[redacted]
R.W. Ashton, Thesis Co-Advisor

[redacted]
W.B. Colson, Chairman
Department of Physics

[redacted]
M. Morgan, Chairman, Department of
Electrical and Computer Engineering

Thesis
567223
c.2

DUDLEY KNOX LIBRARY
NAVAL POSTGRADUATE SCHOOL
MONTEREY CA 93943-5101

ABSTRACT

This thesis is a case study the mechanisms associated with the formation of plasma in a vacuum diode during the break down process. The issues brought forth in this thesis have been studied for many years but have not yet been well understood. Specifically, on the anode of a fast pulsed high vacuum diode the Explosive Electron Emission Model states that the plasma formation is caused by energy deposition on the anode electrode surface. The Desorbed Neutral Ionization model states that the neutral cloud on the anode surface contributes to the plasma formation on the anodic surface. This work presents experimental results which support the model for formation of plasma and thus spot cratering on the anode surface. The findings of the work seem to support the DNI model. However, some of the results are not predicted by the model and it is proposed that the model could be expanded into the study of the behavior of the magnetic fields during the breakdown process.

TABLE OF CONTENTS

I. INTRODUCTION 1

II. THEORETICAL BACKGROUND 3

A. REVIEW OF PLANAR DIODE PHYSICS 3

B. THE FIELD EMISSION 3

C. THE BREAKDOWN PROCESS 5

D. EXPLOSIVE ELECTRON EMISSION MODEL 7

1. Cathode Surface 7

2. Anode Surface 8

E. MECHANISMS CAUSING THE ANODE SURFACE DAMAGE 8

F. PERFORMANCE OF THE EXPLOSIVE ELECTRON EMISSION MODEL..9

III. DESORBED NEUTRAL IONIZATION MODEL 11

A. INTRODUCTION 11

B. DESCRIPTION OF THE DNI MODEL 11

1. Cathode(Ionization Process) 11

C. PLASMA FORMATION 13

D. PREDICTED ONSET OF IONIZATION 15

E. ANODE ELECTRODE 16

IV. SPECIAL ANODE CONSIDERATIONS 21

A. OVERVIEW 21

B. DEFINITION OF AN ANODE SPOT 21

C. ANODE IONS 22

D. MULTIPLE ANODE SPOTS 23

E. ANODE MELTING 24

F. TIMING OF PLASMA PRODUCTION 25

V. EXPERIMENT 29

A. OVERVIEW 29

B. EXPERIMENTAL SET UP 29

1. Equipment and Laboratory Layout 29

2. Diode Current Acquisition Setup 32

3. Anode - Cathode Set Up 34

4. Data Acquisition 37

5. Detection of Anode Damage 38

C. EXPERIMENTAL PROCEDURES 38

1. Marx Generator 38

2. Blumlein Pulse Forming Line 41

3. Electrode Configurations 41

4. Anode Craters Optical Acquisition 44

VI. EXPERIMENTAL RESULTS 46

A. OVERVIEW 46

B. PLASMA FORMATION ON THE ANODE (SET UP 1) 46

C. PLASMA FORMATION ON THE ANODE(SET UP 2) 54

D. PLASMA FORMATION ON THE ANODE (SET UP 3) 59

E. COMPARISON BETWEEN ONE AND TWO 75 KV MARX BANK SHOTS 66

VII. ANALYSIS 78

A. OVERVIEW 78

B. PLASMA FORMATION ON THE ANODE SURFACE.....79

  1. Anode Surface Damage.....79

  2. Formation Of Anode Spots By Unipolar Arcing.....80

C. MULTIPLE ANODE SPOT CRATERS.....80

D. CLUSTER FORMATION.....83

E. POSITIONING OF THE SPOT CRATERS ON THE ANODE SURFACE....83

F. SEQUENCE OF SPOT CRATER PRODUCTION.....88

G. COMPARISON BETWEEN 1 AND 2 SHOTS OF 1 MV DIODE VOLTAGE.....90

VIII. CONCLUSIONS AND RECOMMENDATIONS.....92

APPENDIX. OPERATIONAL PROCEDURES OF PULSERAD 112A.....95

A. PREPARATION OF PULSERAD 112A FOR OPERATION.....95

  1. Set of the Cathode - Anode spacing in the Accelerating tube.....95

  2. Start the Vacuum System.....95

  3. Marx Generator.....96

  4. Charging and Firing the Pulserad 112A.....96

LIST OF REFERENCES.....97

INITIAL DISTRIBUTION LIST.....99

I. INTRODUCTION

Electrical breakdown between charged electrodes and plasma formation on surfaces are fundamental phenomena in many areas of pulsed power technology. Vacuum breakdown in a pulsed high voltage diode is initiated by the explosive-like transition of a field emitting spot into the dense plasma of a cathode spot. These high current, high voltage diodes operate during the time interval between plasma formation and diode gap closure. Even though the electrical breakdown process in diodes has been studied extensively for more than sixty years, the origin of the high current density and the mechanisms which cause the cathode and anode spots have not yet been well understood. A cathode spot produces a crater on the cathode surface through a plasma-related mechanism when a sufficiently strong electrical field is applied on the cold cathode surface.

One widely accepted model used to describe the formation of cathode flares is the whisker explosive electron emission model [Ref. 1]. This model suggests that the electrical field in the diode is enhanced near a microprotrusion or "whisker" on the cathode surface, causing field emission of electrons. The field emitted current supposedly heats the whisker within nanoseconds, until an explosive formation of plasma occurs. There is, however, some doubt as to whether this mechanism can provide enough energy to explode a whisker. A new model developed by Schwirzke [Ref. 2] proposes a more complex process, involving ionization, that can provide the energy required to form the cathode spots.

This work will focus on the pre-breakdown processes that occur in the diode, specifically the plasma formation and the damage that occurs on the anode surface. Previous work in this field at the Naval Postgraduate School confirmed the formation of microscopic craters or spots on both the cathode and the anode surfaces after breakdown. Wright [Ref. 3] suggests that plasma formation on the anode occurs about 1.5 nanoseconds after the initial plasma production begins on the cathode. The study described in this thesis was made using the high voltage vacuum diode of the Naval Postgraduate School Flash X-ray machine. The damage that occurs on the anode surface is described with the aid of an optical microscope, and there is an attempt to explain the mechanisms that made this damage occur.

This study is organized to provide an overview of the breakdown process, to describe the anode surface damage, and then to explain the anode plasma formation. It begins with basic diode physics and theoretical background in Chapter II. Chapter III covers the Desorbed Neutral Ionization Model (Schwirzke), Chapter IV deals with some special topics about the anode, and Chapters V, VI, and VII cover the experiment, results, and analysis, respectively. Chapter VIII offers conclusions and recommendations.

II. THEORETICAL BACKGROUND

A. REVIEW OF PLANAR DIODE PHYSICS

A planar high voltage diode consists of two conducting plates separated by a distance, *d*, which is small relative to the dimensions of the electrodes. The gap between the plates is evacuated, in this case to a vacuum between 10^{-5} and 10^{-6} Torr. In a planar diode where no current flows through the diode gap, the electrical field, *E*, is given by the relationship

$$E = \frac{\Phi_O}{d} \tag{2.1}$$

where Φ_O is the applied voltage potential across the diode. Once a current begins to flow through the diode, the electric field is altered by the changing charge distribution. This is known as "electron space charge effect" (Figure 2.1). The diode used for this experiment was a high voltage diode, for which the potential minimum is very small compared to the high applied potential. This minimum is practically coincident with the cathode surface (Figure 2.1, IV). In this case, the electric field vanishes at the cathode surface. The emitted electrons have approximately zero initial velocity. A sufficient rate of emission causes the electron flow in the high voltage diode to become space charge limited. [Ref. 4]

B. THE FIELD EMISSION

When a sufficiently strong electric field (usually more than 10^7 V/m) is applied across the gap of a vacuum diode, the resulting Lorenz force causes a quantum mechanical tunneling of electrons through the potential barrier binding them to the cathode surface [Ref. 5]. Then the electrons are accelerated toward the anode. This quantum mechanical phenomenon is called field emission.

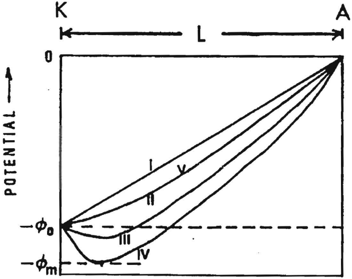

Figure 2.1. Schematic of electrostatic potential in a diode including electron space charge. A time dependent potential minimum forms near the cathode (K) surface. I through IV are sequential in time. [Ref. 4]

This phenomenon occurs at microscopic non-uniformities, dust particles or oxide spots on the cathode surface, which are more commonly referred to as whiskers. The field emitted current density j_{FE} is proportional to the square of the nominal electrical field and is given by the Fowler Nordheim equation:

$$j_{FE} = c_1 \beta^2 E^2 e^{\left(-\frac{c_2}{\beta E}\right)} \qquad (2.2)$$

where β is the electric field enhancement factor and c_1, c_2 are constants based on the work function of the material composition of the cathode electrode. Field emission takes place at the whiskers because their geometry can lead to an electric enhancement from 10 to 100 times the nominal electric field value given by Equation 2.1. The electrical field enhancement can be seen in Figure 2.2.

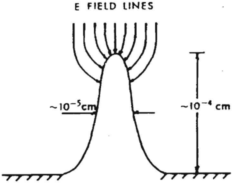

Figure 2.2. Electric field enhancement at a whisker surface. [Ref. 4]

C. THE BREAKDOWN PROCESS

The field emission current is limited by the previously indicated space charge consideration. Using a non-relativistic treatment, which is sufficient for the experiments in this work, the space charge limited current density j_{CL} is given by the Child-Langmuir formula:

$$j_{CL} = \frac{4}{9}\varepsilon_O \left(2\frac{e}{m}\right)^{\frac{1}{2}} \frac{\Phi_0^{\frac{3}{2}}}{d^2} \tag{2.3}$$

where ε_O=8.85 x 10^{-12} F/m is the permittivity of free space, e is the magnitude of charge carried, m is the mass of the charge carriers, Φ_O is the magnitude of the diode potential, and d is the distance from the zero potential surface to the potential Φ_O. Before plasma formation occurs, d is the distance between the electrodes.

The term "breakdown" refers to the filling of the diode gap with a conducting medium, allowing current to flow with little or no resistance. In the vacuum diode, when a high enough voltage is applied across the gap, field emission of electrons takes place at the whiskers and a dense plasma is formed immediately above the electron emitting spots. This occurs a few nanoseconds from the voltage onset. If the plasma occurs above whiskers on the anode surface, it is called an anode flare. If it takes place near the cathode surface, it is a cathode flare [Ref. 1]. The mechanisms by which these flares occur are not completely clear, and there are several theories that attempt to explain these phenomena. The electrical breakdown process is complete when the plasma produced by the anode and cathode flares fills the gap providing the conducting medium in which current can flow freely. This happens a few microseconds after the plasma formation on the electrode surfaces [Ref. 7]. In Figure 2.3, the gap closure which occurs a few microseconds after plasma formation onset is shown [Ref. 6].

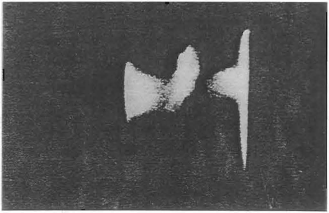

Figure 2.3. This is a time lapsed photograph of a 75 kV shot (typically 1.2 MV peak diode voltage) with a 1 % optical neutral density filter. The bright region near the center shows the collision of the cathode (left side) and anode (right side) plasmas. [Ref. 6]

D. EXPLOSIVE ELECTRON EMISSION MODEL

1. Cathode Surface

A well known model for plasma production on the cathode was proposed by Mesyats *et al.* [Ref. 1]. According to this model, the main mechanism for the formation of the cathode flares begins after the application of the voltage pulse, where there is a field emission of electrons at microprotrusions (whiskers) on the cathode surface. As the applied voltage increases, so will the field emission current density -- until it reaches a value where the ohmic heating will be sufficient to explode these cathode emitting micropoints. There is a very quick vaporization and ionization of the whiskers. This plasmodic material will then expand in an explosive manner at speeds up to 10^4 m/s.

2. Anode Surface

According to Mesyats *et al.*, electrons which have been emitted by cathode flares are accelerated in the vacuum section of the gap, and then transfer their energy to the anode surface. The power flux on the anode for experimental conditions (small diode gap = 0.35 mm, max. voltage = 35 kV, R = 150Ω) is about 10^9 W/cm^2 over 14 ns. If one neglects the heat losses and estimates upper boundaries, it turns out that the energy deposition on the anode surface is sufficient for vaporization of the anode material in an explosive manner, as well as for the formation of anode flares. According to the estimates of Mesyats *et al.*, the mass of metal evaporated from the anode is on the order of 10^{-8} g, i.e., several orders greater than the mass of metal evaporating in a cathode flare. Thus, this model supports the idea that in the final stage the anode can be the main supplier of the conducting medium to the vacuum gap. It also predicts that the anode flares' brightness will be much greater than that of the cathode flares. [Ref. 1]

E. MECHANISMS CAUSING THE ANODE SURFACE DAMAGE

The model proposed by Mesyats *et al.* states that the electron energy that is deposited on the anode surface is absorbed in a layer a few micrometers thick. According to experimental calculations, the rate of heating of the anode surface is almost 10^{10} K/s. The temperature gradient in the surface layer exceeds the value of 10^6 K/cm, so there will be a rapid increase in temperature, which will cause thermal expansion of the heated layer. This will cause significant thermal stresses in the layer. According to Mesyats *et al.*, the craters formed in the breakdown spark process can be considered as solidified-liquid phase elements. This can be explained not only by a purely external analogy, but also by the pattern of the dislocation structure in both the melting and the crater regions. The appearance of craters is related to the presence of microscopic impurities, such as oxides, carbides etc., in the metal surface. Since these impurities have less heat capacity, heat conductivity, and density than metals, there would be localized areas of high temperature in the surface layer. The high temperature causes the appearance of a liquid phase. Based on these ideas, Mesyats' model explains the origin of craters on steel, since they contain carbide inclusions. Thus, craters occur near the grain boundaries where impurities diffuse in the process of metal recrystallization. [Ref. 1]

F. PERFORMANCE OF THE EXPLOSIVE ELECTRON EMISSION MODEL

As explained earlier, once a sufficiently large current begins to flow through the diode, the electrical field distribution is altered by the presence of an "electron emission space charge" and the maximum current density j_{CL} is limited by the Child-Langmuir Law. In general, one would expect that field emission current j_{FE} is less than j_{CL}. Therefore, the Child-Langmuir current to the anode represents an upper limit. For a 1 MV potential applied across a 2.54 cm gap, the Child-Langmuir Law limit in a uniform electric field is $j_{CL}=3.6\text{x}10^6 \text{A/m}^2$. This is far less than density of 10^{12}-10^{13}A/m^2 required to ionize a whisker by joule heating in the 3-10 nanoseconds in which it occurs. [Ref. 2]

The field emission electron current will become space charge limited at a value that is insufficient for the explosive-like transition of the whisker into a dense plasma. Furthermore, the externally applied electrical field vanishes near the cathode surface when the current becomes space charge limited. This should turn off the field emission current. The question remains as to how this relatively small field emission current can cause the formation of a cathode spot in an explosive manner.

III. DESORBED NEUTRAL IONIZATION MODEL

A. INTRODUCTION

The Desorbed Neutral Ionization model (DNI) provides a mechanism that can transfer the amount of energy required to explode a whisker. It also can be applied to help understand the mechanism of plasma formation on the anode. Previous work [Ref. 3 and 7] has demonstrated it to be capable of predicting the delay time between the voltage onset and cathode plasma formation.

B. DESCRIPTION OF THE DNI MODEL

1. Cathode (Ionization Process)

Electrode surfaces are usually far from ultra high vacuum clean. This means that adsorbates like CO_2, O_2 or hydrocarbon molecules are weakly bound to the electrode surface by Van der Waals interactions [Ref. 8]. After the onset of the applied voltage, the resulting current will start to heat the surface. This heating will cause a sudden rise in temperature, especially on the tips of already existing whiskers. This heating, as well as the electrical field, the emission of electrons, and the impact of ions, are all mechanisms which stimulate the desorption of the weakly bound adsorbates from the surface of the whisker. These adsorbates move away from the cathode with an average speed determined by the temperature of the surface. For example, 470 m/s is the average velocity of air molecules at temperature T = 300 K [Ref. 8]. Expanding at this speed, a suddenly released monolayer of 2×10^{19} molecules/m^2 forms a dense gas layer of neutral molecules very close to the cathode surface. As the diode voltage is increased, the energy of the field emitted electrons passing through the neutral gas layer also increases. As soon as the energy of the electrons is high enough that the cross-sectional ionization of the neutrals is sufficient, ionization of the desorbed neutral gas layer will begin. The initial light which signals the onset of plasma formation is believed to be that light produced during the ionization of the neutral gas layer. Figure 3.1 shows a typical ionization cross section as it changes with the energy gained by the electrons as they accelerate away from the cathode surface. It also gives a neutral density profile for the onset of ionization.

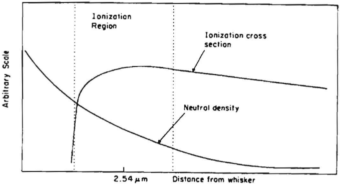

Figure 3.1. Schematic of a typical distribution of ionization cross-section and neutral density. [Ref. 9]

Assuming that the neutrals represent oxygen adsorbates, they will have a maximum cross-section for ionization at about 100 V potential [Ref. 9]. The ionization region is where the ionization cross-section and the neutral density are sufficient to have a reasonable probability for ionization of neutrals. The ionization of the neutrals produces more electrons, which are accelerated to the anode. The corresponding slower moving ions go back to the cathode, where they efficiently transfer energy to the cathode surface, causing more desorption of neutrals. These ions are accelerated toward the tip of the whisker, delivering about 100eV of energy each to the surface layer. [Ref. 10]

C. PLASMA FORMATION

The ion bombardment of the cathode surface caused by the ionization of the neutrals leads to further desorption of neutrals, thus increasing the neutral density. Since ions have larger mass than the electrons, they accelerate toward the cathode at a much slower rate, resulting in the formation of a positive space charge sheath a few micrometers in front of the cathode surface. The presence of this positive space charge increases the electrical field and, through the Fowler-Nordheim relation (Equation 2.2), significantly enhances the field emission current. Also, due to the enhanced electrical field, the 100 V equipotential surface moves closer to the cathode surface into a region of higher neutral density. The continued ionization forms a dense cloud of plasma above the electron emitting spot, which effectively shields the whisker spot from the externally applied electrical field. As the plasma density increases, so does the cathode surface heating (because of the increasing current and the ion bombardment) until thermionic electron emission occurs. This localized build-up of plasma results in pressure gradients and electrical field distributions which help the formation of unipolar arcs [Ref. 10]. Because the external applied field is isolated from the cathode surface, the unipolar arc current density can be much larger than the Child-Langmuir space charge limited diode current density j_{CL}. This high current density, combined with the ion bombardment, is believed to be the basic mechanism that provides the explosive plasma formation and the resulting cathode spots. Some of the craters observed on the cathode surface are shown in Figures 3.2 through 3.4.

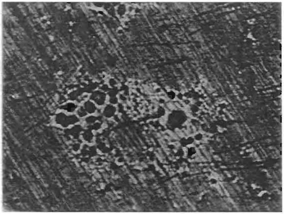

Figure 3.2. Spots observed on the cathode surface after two 75 kV Marx shots. (X 50)

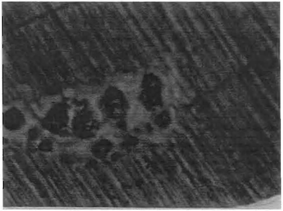

Figure 3.3. Spots observed on the cathode surface after two 75 kV Marx shots. (X 100)

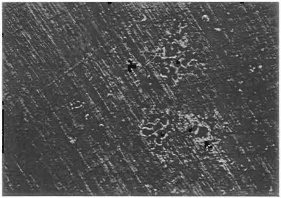

Figure 3.4. Spots observed on the cathode surface after two 75 kV Marx shots. (X 500)

D. PREDICTED ONSET OF IONIZATION

The delay time between voltage onset and plasma formation can be predicted by determining the intersection of a 100 V equipotential surface curve (EPS) and a neutral cloud position curve. [Ref. 2] At the time of intersection, neutral particle density is sufficient for the electrons of 100 eV energy to start the ionization process. Assuming that the cathode and anode surfaces are large compared to the separation distance, *d*, the electrical field between the electrodes is constant, and the location, *x*, from the cathode of a potential, *V(x,t)*, at a time, *t*, is stated by the relation

$$x = \frac{V(x,t)}{\Phi(t)} d \tag{3.1}$$

where $\Phi(t)$ is the potential applied to the anode and *d* is the separation distance between the electrodes. With the use of Equation 3.1, it is possible to plot the 100 V equipotential surface curve for a 75 kV Marx shot, which corresponds to 1.04 MV inside the diode. It can also be combined with the neutral distance curve, which is a linear plot of position based on an average velocity of 470 m/s. (Figure 3.5) So, for instance, it is possible to predict that the onset of ionization of the neutral cloud for a 75 kV Marx shot begins about 8.5 nanoseconds after the voltage onset.

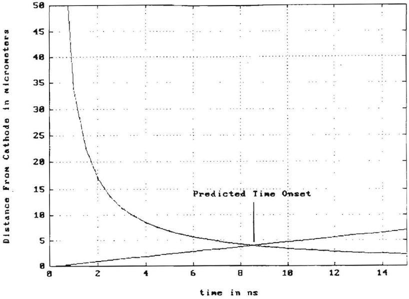

Figure 3.5. Equipotential surface of 100 V and distance of neutrals from the cathode vs. time from voltage onset. Assumed pulse rise time is 20 ns.

E. ANODE ELECTRODE

In the past [Ref. 11] and in the course of the present work, small craters on the anode surface (anode spots) have been observed. These spots are believed to be produced by the same mechanisms that are responsible for craters on the cathode surface. Since the anode surface is covered with adsorbates, the energetic electrons coming from the cathode region will strike these adsorbed neutrals, causing their ionization. When the electron flux and neutral density on the surface become sufficient, a strong ionization rate will result. This causes the formation of a positive space charge layer a few micrometers from the anode surface. The potential of the ion layer will be increased, and becomes greater than the applied field in front of the anode. This is due to the larger mass and the larger inertia of the ions. The time of flight of the ions to the cathode is approximately 10 ns, which is much longer than the time it takes a secondary electron to travel the few micrometers to the anode surface. The field then reverses, and unipolar arcing will occur. The ion density above the anode surface that is required to sustain field reversal is given by the relation

$$E = \frac{\sigma}{\varepsilon_o} \tag{3.2}$$

where ε_o is the permittivity constant and σ is the ion space charge layer density (C/m^2). If the applied voltage at the moment of breakdown was 250 kV over a 2.5 cm diode gap, the electrical field E = 10^7 V/m. Field cancellation will occur if $\sigma = E\varepsilon_o = 8.85$ x ^{10} C/m^2. This means that the density of the ion layer will be $d_i = \sigma/q_i = 5.52 \times 10^{14}$ ions/m^2, where q_i=1.6022 x 10^{-19} C. If a field reversal with an electrical field of $E = -10^7$ V/m is desired, it is necessary to have twice the value of d_i or 1.1 x 10^{15} ions/m^2. When the density of the ions at the ion layer reaches this value, the plasma layer formation in the region in front of the anode and unipolar arc can take place. The ionization rate created by the high energy electrons is estimated under the assumption that the electron current density is limited by the Child-Langmuir Law. Applying Equation 2.3, the current density j_{CL} =0.45 X 10^6 A/m^2 for E = 250 kV over a 2.5 cm diode gap is obtained. This corresponds to an electron flux of Φ_e =2.8 x 10^{24}e$^-$ / (m^{2}s). For a typical delay time of 10 nanoseconds, the neutrals will have traveled with a velocity of 470 m/s a distance of 4.7 micrometers from the anode surface. The average number of molecules in one adsorbed monolayer is estimated at 2.2 x 10^{19} particles/m^2 [Ref. 3]. Since the anode area is 4.5x 10^{-3}m^2, the average number of neutrals if one monolayer is desorbed will be N = 9.9 x 10^{16} particles in a volume of V = 2.11 x 10^{-8} m^3. So, the average neutral density n_o = N/V = 4.7 x 10^{24} particles/m^3, which is about one-fifth the density of air at atmospheric pressure. With this average density of the neutral cloud, the electrons' mean free path will be λ = 1/ $n_o\sigma_c$, where σ_c is the cross-section of ionization. For many gases, σ_c ~ 10^{-22} m^2 [Ref. 9]. So, λ = 1/ $n_o\sigma_c$ = 2 x 10^{-3} m. This means that the 2x10^{-3} distance of the mean free path is long in comparison to the dimension of the neutral cloud of 4.7 μm. The ionization rate is R_{ion} = η Φ_e, where η is the efficiency of ionization, or η=4.7 x 10^{-6} / λ= 2.35 x 10^{-3} ionizations / e^-. This gives an ionization rate of R_{ion} = 6.58 x 10^{21} ionizations /(m^{2}s). At this rate, it would take abut 16 nanoseconds to create an ion layer of 1.1 x 10^{15} ions / m^2, which is required for field reversal. This estimate shows that the high energy electron current density may not be quite able to cause sufficient ionization of the neutral cloud in front of the anode surface to create a field reversal. Therefore, it is possible that there are other ionizing mechanisms which contribute to the field reversal. It is believed that there could be two other ionization mechanisms. One is radiation (especially in the ultra violet band) created by the cathode plasma. Unfortunately, at this time there is no way to estimate the amount of the ionizing radiation. The other ionization mechanism is driven by the back scattered and less energetic secondary electrons produced during the ionization process. These secondary electrons are slower than the high energy electrons, so they will ionize the neutral gas cloud more efficiently. Secondary electrons are produced by ionization a few micrometers from the anode surface at a region with a potential of about -100 V with respect to the anode. They are accelerated towards the anode, and their ionization cross-section is much higher, by about two orders of magnitude $\sigma_C \sim 10^{-22}$ m^2 than that of the high energy electrons. Their mean free path is correspondingly much smaller [Ref. 7]. This means that the secondary electrons could be considered to be a very significant source of ionization for the desorbed neutral gas layer and the still adsorbed neutrals on the anode surface. Figure 3.6 shows a schematic of the ionization process sustained by secondary electrons.

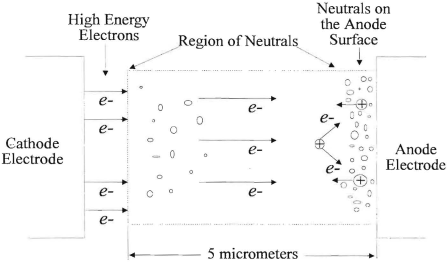

Figure 3.6. Ionization process in front of the anode surface sustained with secondary electrons.

IV. SPECIAL ANODE CONSIDERATIONS

A. OVERVIEW

In order to support the theory used in this study it is essential to present what other researchers have reported about the same phenomena. In this chapter the experimental findings of other researchers as Miller [Ref. 12 and 13] are summarized. Most of these experiments were performed on relatively long time scales (on the order of ms) while the current experiments investigate the formation of anode spots on a 10 ns time scale.

B. DEFINITION OF AN ANODE SPOT

In discussing anode spots, one must be careful in making conclusions regarding exactly when an anode spot is present. It has been suggested that, since anode spots are very luminous, someone could judge the appearance of anode spots by examining the luminosity of the anode. That would not be satisfactory, since luminosity can be affected by plasma radiation and, of course, the detector's sensitivity. Therefore, a luminous area on the anode does not define an anode spot. On the other hand, since an anode spot is always bright, the absence of a bright spot on the anode could be considered to be conclusive evidence that an anode spot is not present. Miller [Ref. 12] states that most researchers have found the formation of a large area anode spot to coincide with a significant decrease in the voltage noise component, and usually with a decrease in the mean diode voltage. Thus, a significant decrease in the diode voltage noise component, especially if accompanied by the appearance of a very luminous spot on the anode surface, could be assumed to indicate the formation of a large anode spot plasma.

However, the formation of microsized anode spots caused by unipolar arcing could take place without any decrease of the voltage noise. In this case, identification of the formation of anode spots on the anode surface would require that the suspected anode spot not only be very luminous, but also a source of significant erosion on the anode electrode surface. [Ref. 12]

C. ANODE IONS

There have been many published works on ion production processes in the region of the anode electrode. Kimblin [Ref. 14], while working with vacuum arcs, found that significant quantities of anode ions were emitted from dc arcs. He has also reported that the positive ion current constitutes 7 to 10 percent of the total arc current for a wide variety of cathode materials [Ref. 15]. When an anode spot is present, the fractional positive ion flux increases significantly. Kimblin's work with various materials like copper, chromium, and tungsten gave comparable results for the maximum ion currents. The anode ion flux appears to be a linear function of the arc current, and thus behaves much like the cathode ion flux. The anode ion flux starts from zero at the critical current for anode spot formation and then increases more rapidly than the cathode ion flux. As mentioned earlier, the Desorbed Neutral Ionization (DNI) model assumes that there is a neutral layer on the anode surface which is struck by the huge flux of electrons from the cathode. This neutral layer is ionized, forming a positive sheath a few micrometers from the anode surface. Ions are pulled toward the cathode. Kimblin compared the measured anode erosion rate with the anode ion current and found that much of the anode material was ionized. Bacon [Ref. 16] also found anode plasma to be highly ionized. This indicates that a significant fraction, if not the majority, of the material eroded from the anode by the anode spot leaves the anode region as ions. [Ref. 12]

D. MULTIPLE ANODE SPOTS

During the course of this work, numerous microsized craters (spots) were observed on the anode surface, as is discussed in Chapter V. Yokohama and Kashitani [Ref. 17] have also observed the presence of several anode spots during the application of 50 Hz vacuum arcs on copper electrodes. Frind and others [Ref. 18] used rectangular current pulses, and showed that at 10 kA, numerous small anode spots, covering a small, well-defined area of the anode, became visible early (in the first few hundred microseconds) in the arc. The vapor emission of these spots was so strong that from 0.4 ms on, they were hidden behind a cloud of plasma. At higher current values, this process occurred more rapidly, and an anode plasma formed. It was tentatively concluded [Ref. 18] that the discrete small anode spots gradually coalesced to form a single, large, rather homogeneous anode spot.

Zycova and others [Ref. 19] also used rectangular current pulses ($I < 4000$ A, 1.8 ms $< t <$6.5 ms) using various electrode materials (Cu, Sn, W, Ag and Zn). They worked mainly with gas discharges and made some interesting observations at pressures of 10^{-4} Torr. Specifically, they observed a cluster of individual spots on the anode electrode surface. The individual spots had diameters around 0.01 mm, while the diameter of the cluster was about ten times larger (about 0.1 mm). They also observed that the anode spots were more constricted on electrodes of higher thermal conductivity. This behavior was attributed to the need to maintain a plasma temperature high enough to produce the necessary current carriers in the anode electrode region. Small anode spots were also observed by Grisson and Newton in their work with physically small anodes [Ref. 20]. Their anode spots tended to be about 10 μm in diameter, and they also observed that several such anode spots were present simultaneously. The fraction of the anode area covered by anode spots increased when the total number was increased. These anode spots never joined to form a single large spot. This is in agreement with the results of the current effort, as can be seen in Figure 4.1, and as further discussed in the following chapters.

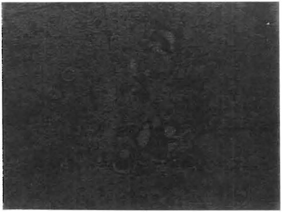

Figure 4.1. Anode spots observed during the present work. (X500)

E. ANODE MELTING

Anode melting in a vacuum anode is generally connected with the formation of an anode spot. The anode electrode surface temperature for a fully developed anode spot has been determined to be near the boiling temperature of the anode electrode material [Ref. 21]. Rich and others [Ref. 21] have found that anode spot formation and anode melting coincide within their experimental resolution (approximately 20-30 milliseconds) for most of the investigated materials. However, melting of the anode is not necessarily correlated with the formation of an anode spot. In the past, there were reports of cases where anode melting occurred without the appearance of an anode spot [Ref. 21]. The answer to this problem may be found, in part, in the behavior of the diode-arc voltage. Goldsmith [Ref. 22] states that the transition of the arc to the anode spot mode is generally marked by the appearance of a significant oscillatory component on the arc voltage. The melting of the anode results from the energy flux into it, carried by an electron and ion current. Goldsmith cites several combinations of cathode and anode materials used in order to determine the threshold peak current I_{pt} for the onset of the anode surface melting. The melting of the anode surface took place only when the peak value of the arc current, i_{peak}, was greater than the threshold peak current I_{pt}. Experimental results show that the threshold peak current I_{pt} depended on both the anode and the cathode materials. Goldsmith's work also supported the theoretical implication that the threshold peak current I_{pt} is inversely proportional to the effective anode potential ϕ_E. Experimental evidence also suggested that the emission of anodic atoms takes place from the onset of the discharge, and is significantly increased when melting of the anode is observed. [Ref. 23]

F. TIMING OF PLASMA PRODUCTION

As mentioned earlier, the purpose of this work is to investigate plasma formation and the resulting damage to the anode electrode surface. To place this in context, it is helpful to summarize the results of some previous related work at the Naval Postgraduate School.

Wright [Ref. 3] worked on the time of plasma production in both the electrodes of cathode and anode. Using photodetectors, he observed the difference between the onset of the diode voltage and the onset of light on the diode electrodes. In Figure 4.2, the diode voltage for a 75 kV Marx shot can be seen as a function of time, where the onset is at 33 ns. The light signal for a 75 kV Marx Shot is pictured in Figure 4.3. The "75 kV Marx shot" indicates that the 12 stages of the Marx shot generator are loaded with 75 kV each. A 75 kV Marx shot typically corresponds to 1.04 MV peak diode voltage. Onsets for both the cathode and anode light signals occur at about 40 ns. There is a measured delay time of about 7 ns. This agrees with the predicted delay time of 7.5 ns, according to the DNI model. Wright also concludes that the light signal produced near the cathode surface during the onset is brighter, and begins before the first light emanating from the anode region. This confirms that the cathode process starts and controls plasma production in high pulsed vacuum diodes.

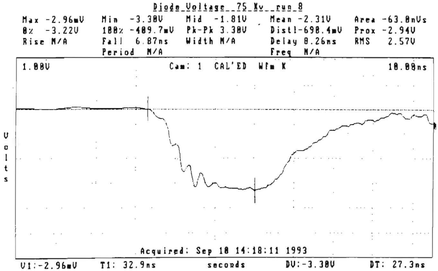

```
                         Diode_Voltage__75_Kv__run_8
Max -2.96mV   Min   -3.30V    Mid   -1.81V    Mean -2.31V     Area -63.0nVs
0%  -3.22V    100% -409.7mV   Pk-Pk 3.30V     Distl-690.4mV   Prox -2.94V
Rise N/A      Fall  6.07ns    Width N/A       Delay 0.26ns    RMS   2.57V
              Period  N/A                     Freq  N/A
1.00V                      Cam: 1  CAL'ED  Wfm K                    10.00ns
                       Acquired: Sep 10 14:18:11 1993
V1:-2.96mV    T1: 32.9ns          seconds         DV:-3.30V        DT: 27.3ns
```

Figure 4.2. Diode voltage for a 75 kV Marx shot (1.2 MV peak diode voltage). The onset of voltage starts at 32.9 ns. [Ref. 3]

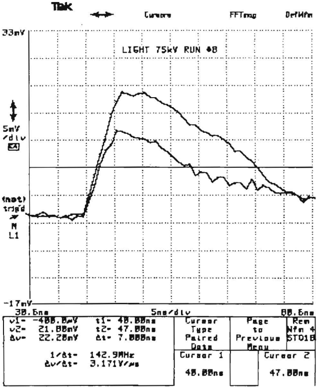

Figure 4.3. Light signals for a 75 kV Marx Shot (1.2 MV peak diode voltage). The onset of the light for both anode and cathode signals starts at 40 ns. This means that there is a delay of 7 ns between the onset of the light and the onset of the diode voltage. [Ref. 3]

V. EXPERIMENT

A. OVERVIEW

This work is intended to study the formation of plasma; specifically the damage mechanisms which cause the formation of craters on the surface of the anode electrode, the geometry of the damage, and the condition of the electrodes used. The damage on the anode electrode is compared with the Desorbed Neutral Ionization model described in Chapter III.

B. EXPERIMENTAL SET UP

1. Equipment and Laboratory Layout

This experiment was performed at the Naval Postgraduate School (NPS) Flash X Ray (FXR) facility using a Physics International Company Pulserad 112A flash x-ray machine. The Model 112A Pulsed X-Ray Generator is a high power flash x-ray and electron accelerator system. It is specifically designed for radiation effects studies producing x-ray intensities exceeding 5×10^{10} Rad/sec. Some of the system characteristics, as listed in the Operations and Maintenance Manual [Ref. 24], are provided in Table 5.1. A schematic of the system is shown in Figure 5.1.

The Pulserad 112A uses a high vacuum diode (between 10^{-5} and 10^{-6} Torr) with a diode gap of 2.5 cm. Across this diode the Pulserad 112A generates voltage pulses with a duration of 20 to 25 nanoseconds at full width half maximum (FWHM). The amplitude of the potential applied inside the vacuum diode can vary between 600 kV and 1.6 MV. The anode and the cathode used in the study were made from stainless steel. The Pulserad 112A system consists of five basic subassemblies:

1. DC power supply and controls
2. Trigger system
3. Marx generator
4. Coaxial pulse generator
5. Electron accelerator tube.

Marx Generator		
	Stages	12
	Stage Capacitance	. 05 mF
	Output Capacitance	4. 7 nF
	Maximum Charge Voltage	100 kV
	Maximum Stored energy	3000 J
Blumlein Generator		
	Output Impedance	43 Ohms
	Output Voltage	1. 7 MV
	Output Pulse Width (FWHM)	20 ns
X - Ray Output		
	Dose At 0. 5 Meters From Anode	8 R
Power Requirements		
	Power Supply	220 Vac, 50 /60 Hz, 500 VA max.

Table 5.1. System characteristics of Pulserad 112A. [Ref. 24]

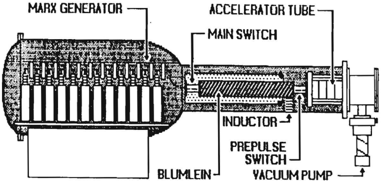

Figure 5.1. Layout of the FXR facility. [Ref. 25]

The basic theory of operation will be summarized below. The Pulserad 112A functions following three basic steps. The Marx Generator is charged via an external power supply to the desired voltage. The Blumlein Pulse Forming Line is then resonantly charged from the Marx generator. Then, the fully charged Blumlein, discharges rapidly into the electron accelerator tube creating a large potential difference across the diode gap. When the high voltage is applied, the stainless steel cathode rod emits electrons which are accelerated across the anode-cathode spacing until they impact with a stainless steel target (anode). There is also a triggering system which controls the charging and discharging phases of the operation. This triggering system consists of numerous gas spark switches which close as a result of the electrical breakdown of the pressurizing gas. For a complete description of the Pulserad 112A refer to Reference 24. The diode current was measured using installed monitors supplied with the Pulserad. The signals from these monitors were measured by a Tektronix 7104 1 GHz oscilloscope and Tektronix Digital Camera System (DCS). The diode current signal required 20 dB attenuation to be viewed on the oscilloscope. The absolute magnitudes of these signals can be obtained using the oscilloscope trace. Actual diode current is determined by:

$$I_{ac}\ [\mathrm{kA}] = 7.31 \times V_{scope} \tag{5.1}$$

where V_{scope} is the voltage read from the oscilloscope in volts. [Ref. 6]

The measurement and detection equipment used in this study, along with its most important operating characteristics, is listed in Table 5.2.

Equipment	Purpose	Model	Characteristics
Fluxmeter	Current Detector	Physics International / PIM 199B	0. 872 kV /T sensitivity) 5% Accuracy
Voltage Divider	Detect / Send Voltage Pulse	Physics International / PIM - 197A25B	1. 6 kV / v Sensitivity) 5 % Accuracy
Oscilloscope (2)	Acquires Voltage and Current Waveforms	Tektronix/ 7104 w/7B92A	Time Base 1 GHzBW) 3 %
Digitizing Camera System	Measures and Records Oscilloscope Waveforms	Tektronix/ DCS 01	512 Pixels / Sweep Use w / 7104 Scopes
Digitizing Signal Analyzer	Acquires, Measures and Records Light and X - Ray waveforms	Tektronix/ DCA 602A w /11A34 Plug In	1 GHzBW(2 Channel) Disk Drive storage Spreadsheet Files) 0.03 % Timebase Accuracy
Optical Microscope	Detect / photoanode surface craters	Zeiss ICM 405	Magnifications X 50, 100, 200, 500, 1000

Table 5.2 Detection and measuring equipment used for experiment

2. Diode Current Acquisition Setup

The light signal produced at the anode and cathode is converted into an electrical signal using two New Focus Model 1601 photodetectors. The produced electrical signal can then be recorded by the Tektronics digital system DSA 602A. In order to eliminate electromagnetic noise, the detectors are housed in a 1.25 cm thick aluminum barrel. The outputs are connected to a high frequency capable, heavily shielded, coaxial cable. The two fiber optic bundles, each 0.318 cm in diameter and 183 cm long, have one end coupled to the photodetector's optically sensitive area. The other end is fed through drilled holes of a lead brick. The lead bricks are necessary to prevent x-rays from registering on the light detectors. The ends of the fiber optic cables are then separated by a 7 mm thick aluminum plate which is placed flush against the vacuum chamber window and centered on the middle of the diode gap. This plate serves to block light produced on the cathode surface from entering the fiber optic cable positioned to receive light from the anode, and vice versa. Only the diode current signal is recorded for this experiment. The configuration of the optical setup is shown in Figure 5.2.

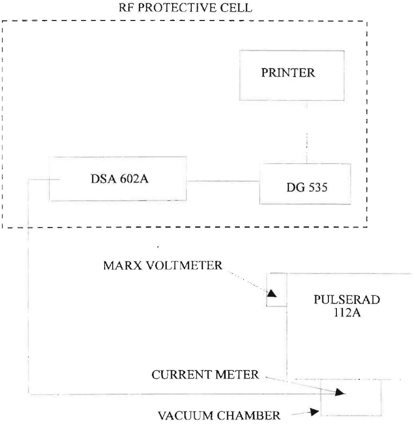

Figure 5.2. Configuration of Diode Current Acquisition Setup.

3. Anode - Cathode Set Up

In this experiment three pairs of stainless steel anodes and cathodes are used. The surface of each anode is thoroughly polished before every use in order to avoid any surface roughness, which could influence the plasma formation. The schematic of the stainless steel anode can be seen in Figure 5.3. The surface of every cathode is also polished before each use for the same reason as for the anode. The schematic of stainless steel cathode can be seen in Figure 5.4. Photos of the cathode and anode surfaces can be seen in Figures 5.5 and 5.6, respectively.

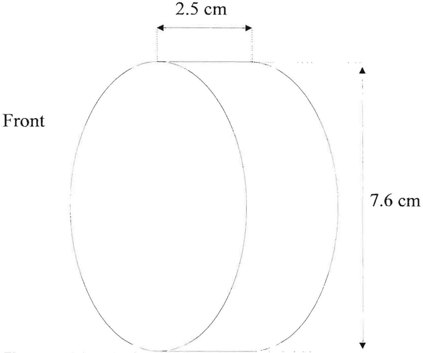

Figure 5.3. Schematic of anode stainless steel electrode.

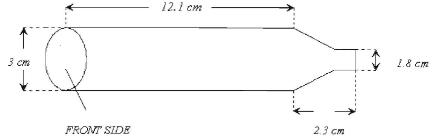

Figure 5.4. Schematic of cathode stainless steel electrode.

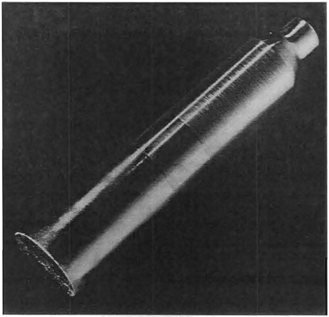

Figure 5.5. Photo of cathode stainless steel electrode.

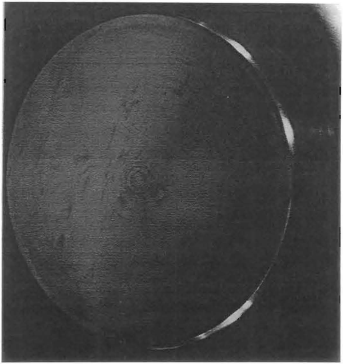

Figure 5.6. Photo of anode stainless steel electrode.

4. Data Acquisition

To obtain the desired waveform of the diode current, the Marx Bank capacitors are charged in parallel and then discharged in series across the diode gap. This is accomplished using the following procedure:

1. Turn on the oscilloscopes / DSA 602A device.
2. Set the pressures on the control switches in accordance with the pressure charts.
3. Charge the Marx Bank turning on all proper switches.

4. After the Marx Bank is charged to the desired voltage of 75 kV the red light will come on. Press the trigger button and the voltage will be released across the diode. Then the waveform of the diode current will appear on the oscilloscope / DSA 602A.

5. Detection of Anode Damage

The detection of the damage being caused on the surface of the anode electrode is achieved and photographed using an electron-microscope Zeiss ICM 405 being held at the Laboratories of the Department of the Material Science of the Naval Postgraduate School.

C. EXPERIMENTAL PROCEDURES

The operating instructions of the Pulserad system are given in the Appendix. Here the role of the two most important parts of the system, the Marx Generator and the Blumlein transmission line, are summarized. A more complete description of the Pulserad 112A is given in [Ref. 23].

1. Marx Generator

Marx Generator is a system which consists of a number of capacitors which are charged in parallel and discharged in series producing high output voltages. Various switches control the discharge of these capacitors. A four stage Marx generator is represented in Figure 5.7. Each capacitor is charged by a DC power supply with a voltage V_O. Triggering of the switches connects the capacitors in series, resulting in an output voltage four times the original charging voltage [Ref. 25]. The Marx generator of the Pulserad 112A consists of twelve stages. Each stage contains two 0.1 microfarad capacitors in series, resulting in a total stage capacitance of 0.05 microfarads. A full schematic of the Pulserad 112A Marx Generator is given in Figure 5.8. The resistors of the system have the advantage that they are capable of high power dissipation and are flexible enough to be easily contoured to fit the electrical requirements of the system generator.

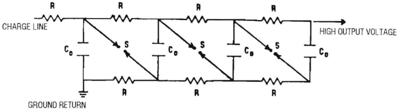

Figure 5.7. Schematic of a four stage Marx Generator. [Ref. 25]

The Marx Generator has the properties of a capacitor with 1/12 the capacitance of a single stage. The output capacitance is given in [Ref. 24] by

$$C_{output} = (1/12) \times 0.\ 05\ \mu F = 4.17 \text{ nF}$$

The output voltage of the Generator becomes 12 times the charging voltage of a single stage. This means that

$$V_{output} = 12 \times Vo$$

where V_O is the DC charging voltage of the capacitors.

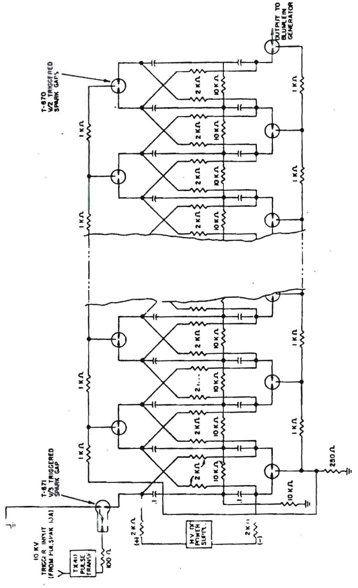

Figure 5.8. Schematic of the Marx Generator of the Pulserad 112A. [Ref. 24]

2. Blumlein Pulse Forming Line

The Pulserad 112A uses a Blumlein transmission line that is resonance charged by the Marx Generator. The use of this line results in a decrease in pulse duration and a corresponding increase in output power. For this experiment, the desired voltage is 75 kV. The Blumlein pulse charge voltage is given by the relation [Ref. 24]:

$$\text{Bl. Volt.} = 12 \text{ x } 1.2 \text{ x } .9 \text{ x Marx Voltage.} \qquad (5.2)$$

For present purposes,

$$\text{Bl. Volt.} = 12 \text{ x } 1.2 \text{ x } .9 \text{ x } 75 = 972 \text{ kV.}$$

In [Ref. 23] the diode voltage is given by

$$V_{diode} = 2 \text{ x Bl. Volt. x } (50/93),$$

where the factor (50/93) expresses the impedance of the circuits of the system. Thus, for the present experiment

$$V_{diode} = 2 \text{ x } 972 \text{ x } (50/93) = 1.04 \text{ MV.}$$

3. Electrode Configurations

There were used three configurations of the anode and cathode electrodes in this experiment. In the first configuration, which can be seen in Figure 5.9, two shots of Marx voltage 75 kV were used to determine the plasma formation by detecting the damage occurred on the anode surface.

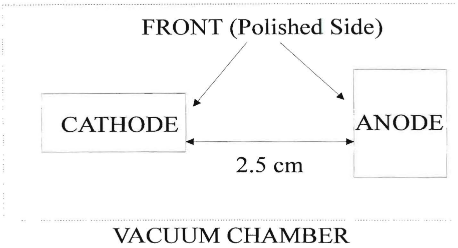

Figure 5.9. Schematic of the first anode cathode configuration

In the second configuration, which can be seen in Figure 5.10, a pair of polished anodes and cathodes that were suitably marked were utilized in order to observe any geometrical relation between the damage on the anode electrode and the cratering on the cathode electrode surface. There was one shot of Marx voltage of 75 kV inside the diode of the FXR machine.

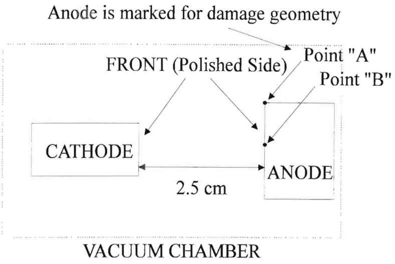

Figure 5.10. Schematic of the second anode-cathode configuration.

In the third configuration, a cathode that was polished and an anode which was half polished were used (see Figure 5.11). They were again marked in order to provide information about the geometry of the effects being observed on the surface of the anode electrode. There was a series of three firings of 75 kV inside the diode of the FXR machine.

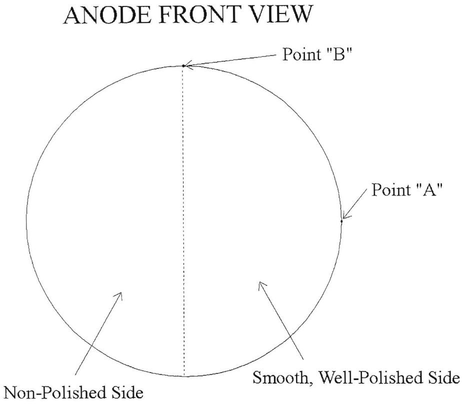

Figure 5.11. Schematic of the anode surface in the third anode-cathode configuration.

4. Anode Craters Optical Acquisition

A crucial part of the experiment is to detect any damage occurring on the anode electrode surface. This meant that the questions to answer are, "Do anode spots exist? Does plasma form on the anode surface?" In order to make specific observations on the anode surface, the optical microscope Zeiss model ICM 405 is employed [Ref. 26]. This enables photos of anode regions magnified 50, 100, 200, 500 and 1000 times to be obtained. Thus, sufficient data is gathered to prove the existence of anode spots and plasma formation in front of the anode electrode surface.

VI. EXPERIMENTAL RESULTS

A. OVERVIEW

In an effort to determine the plasma formation and the damage occurring on the surface of the anode electrode three set ups of anode and cathode electrodes are used. The experiment is performed at a Marx charge voltage potential of 75 kV which corresponds theoretically to 1.04 MV across the diode. The damage caused on the anode surface is detected, observed, and photographed with the use of an optical microscope Zeiss ICM 405. The results recorded in this chapter are discussed according to which setup was employed. Additionally, experimental results will also be discussed in further detail in Chapter VII.

B. PLASMA FORMATION ON THE ANODE (SET UP 1)

In the first electrode set up there is only one 75 kV Marx Bank discharge. The position of the electrodes is marked in order to provide geometric information about the relation between plasma formation on the anode and the corresponding phenomena on the cathode electrode surface. The damage and cratering occurring on the anode electrode surface are shown below in Figures 6.1 through 6.14. The diode current signal is also detected with this single shot, and is shown in Figure 6.16.

Figure 6.1. Photograph of anode surface after one 75 kV Marx bank shot. Note the concentration of craters in a region with many scratches. (X50)

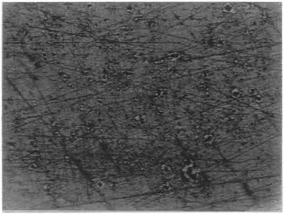

Figure 6.2. Photograph of anode surface after one 75 kV Marx bank shot. Large number of anode craters occurs in a non-uniform way. (X100)

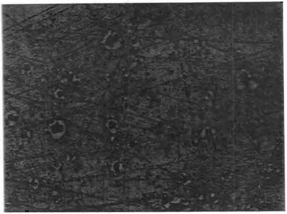

Figure 6.3. Photograph of anode surface after one 75 kV Marx bank shot. Some of the craters emerge on scratches but some do not. (X200)

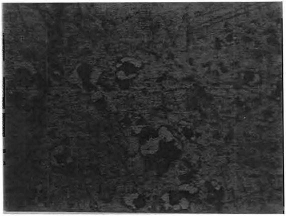

Figure 6.4. Photograph of anode surface after one 75 kV Marx bank shot. Note the different scheme of the anode craters. (X 500)

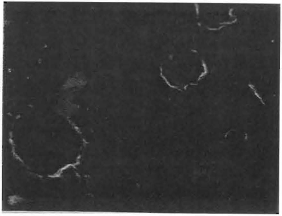

Figure 6.5. Photograph of anode surface after one 75 kV Marx bank shot. Circular craters emerge on the anode surface. (X1000)

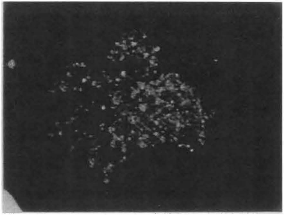

Figure 6.6. Photograph of anode surface after one 75 kV Marx bank shot. Note the huge cluster and the rotation of its "legs". (X 50)

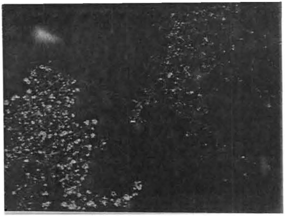

Figure 6.7. Photograph of anode surface after one 75 kV Marx bank shot. Two huge clusters are separated by undamaged surface. (X 50)

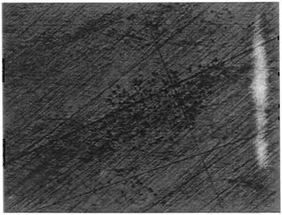

Figure 6.8. Photograph of anode surface after one 75 kV Marx bank shot. There is a concentration of anode craters at the intersection of two deep preexisted scratches. (X50)

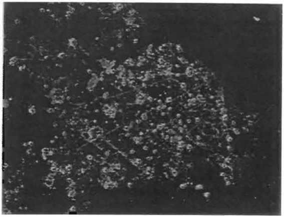

Figure 6.9. Photograph of anode surface after one 75 kV Marx bank shot. A cluster consisting of many anode craters is present, while beside it there is no damage. (X 100)

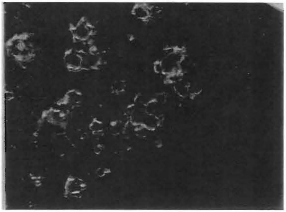

Figure 6.10. Photograph of anode surface after one 75 kV Marx bank shot. Note the large damage occurred on half of the photo while on the other half the anode surface appears undamaged. (X 500)

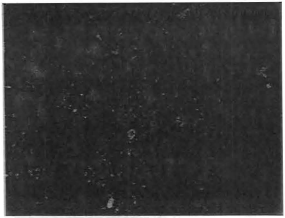

Figure 6.11. Photograph of anode surface after one 75 kV Marx bank shot. Note the huge cluster. (X50)

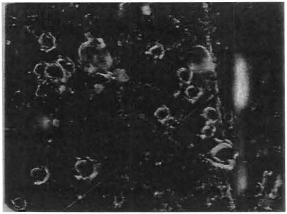

Figure 6.12. Photograph of anode surface after one 75 kV Marx bank shot. This is a detail view of the huge cluster seen in Figure 6.11. (X 500)

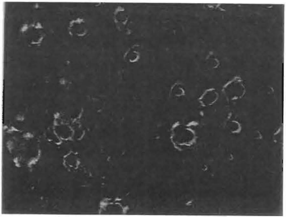

Figure 6.13. Photograph of anode surface after one 75 kV Marx bank shot. Note the non-uniformity of the crater formation. (X 500)

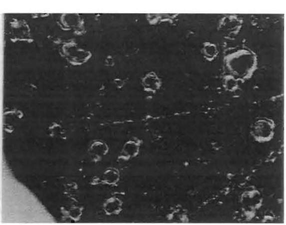

Figure 6.14. Photograph of anode surface after one 75 kV Marx bank shot. Note that the damage caused by cratering occurred in a non-uniform way. (X500)

C. PLASMA FORMATION ON THE ANODE(SET UP 2)

Two 75 kV Marx Bank shots are released during the first set up in order to detect the plasma formation on the anode surface. The damage and cratering occurring on the anode electrode are shown below in Figures 6.15 through 6.23.

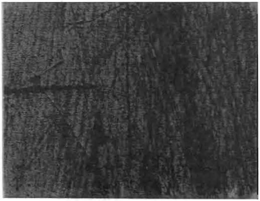

Figure 6.15. Photograph of anode surface after two 75 kV Marx bank shots. Note the series of anode craters along a preexisting scratch. (X 50)

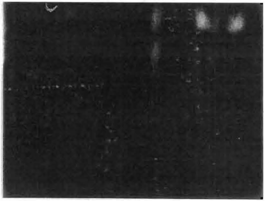

Figure 6.16. Photograph of anode surface after two 75 kV Marx bank shots. Note the impressive serial order of anode craters. (X 50)

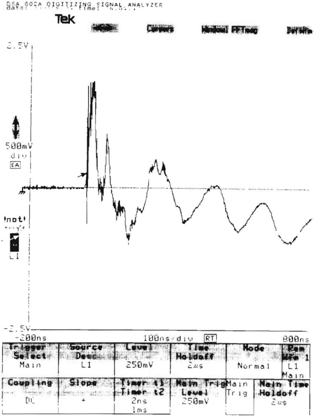

Trigger Select: Main
Source Desc: L1
Level: 250mV
Time Holdoff: 2µs
Mode: Normal
Rem Wfm 1: L1 Main
Coupling: DC
Slope: +
Timer t1 Timer t2: 2ns 1ms
Main Trig Level: 250mV
Main Trig
Main Time Holdoff: 2µs

Figure 6.17. The waveform of the diode current after one 75 kV Marx bank shot.

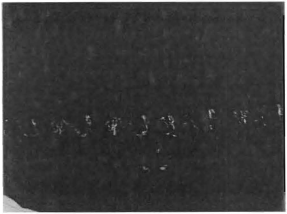

Figure 6.18. Photograph of anode surface after two 75 kV Marx bank shots. Note the line of anode craters. (X 200)

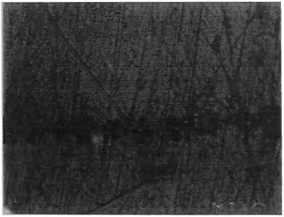

Figure 6.19. Photograph of anode surface after two 75 kV Marx bank shots. This is the same target area as seen in Figure 6.18, but with lower exposure. Note the line of anode craters along this scratch, while along other scratches there are no craters. (X200)

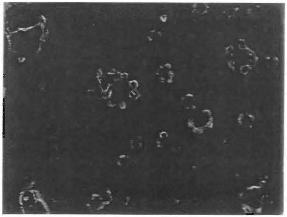

Figure 6.20. Photograph of anode surface after two 75 kV Marx bank shots. Note the explosive manner of the formation of craters. (X 500)

Figure 6.21. Photograph of anode surface after two 75 kV Marx bank shots. Damage has occurred in a scratched area. (X 500)

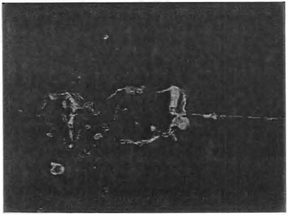

Figure 6.22. Photograph of anode surface after two 75 kV Marx bank shots. Note the significant damage which has occurred along a preexisted scratch. (X500)

Figure 6.23. Photograph of anode surface after two 75 kV Marx bank shots. Note the various sizes of craters occurring in a non-uniform way on the anode surface. (X 500)

D. PLASMA FORMATION ON THE ANODE (SET UP 3)

Figures 6.24 through 6.36 show the damage caused on the anode surface after three 75 kV Marx Bank shots on the stainless steel anode surface. Here the anode electrode is half polished, as mentioned earlier, and each figure denotes whether the image is of the polished or unpolished side.

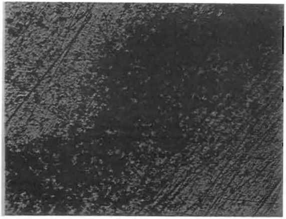

Figure 6.24. Photograph of anode surface after three 75 kV Marx bank shots -- polished side. Note the large concentration of craters in this particular area on the anode surface. (X50)

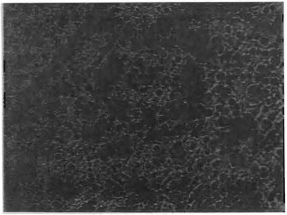

Figure 6.25. Photograph of anode surface after three 75 kV Marx bank shots -- polished side. Note the concentration of damage. (X200)

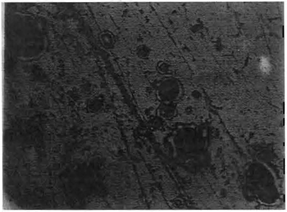

Figure 6.26. Photograph of anode surface after three 75 kV Marx bank shots-polished side. Note that some of the craters occur on an unscratched surface. (X500)

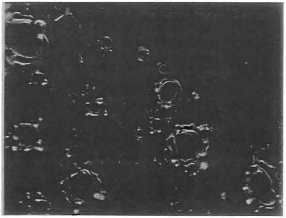

Figure 6.27. Photograph of anode surface after three 75 kV Marx bank shots -- polished side. Note the large non-uniform craters. (X500)

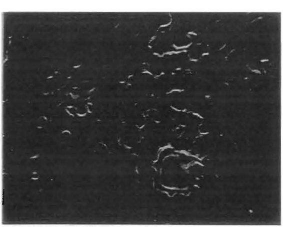

Figure 6.28. Photograph of anode surface after three 75 kV Marx bank shots -- polished side. Note the large concentration of craters. (X500)

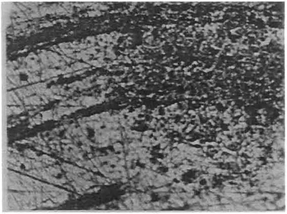

Figure 6.29. Photograph of anode surface after three 75 kV Marx bank shots -- unpolished side. Note the rings of the anode surface and the cluster of craters covering them. (X100)

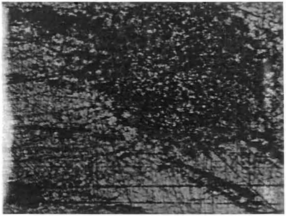

Figure 6.30. Photograph of anode surface after three 75 kV Marx bank shots -- unpolished side. Note the concentration of craters in a cluster. (X500)

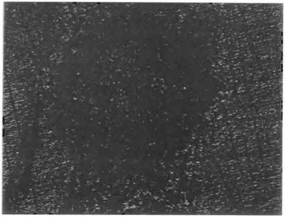

Figure 6.31. Photograph of anode surface after three 75 kV Marx bank shots -- unpolished side. Note the cluster surrounded by a less damaged area. (X100)

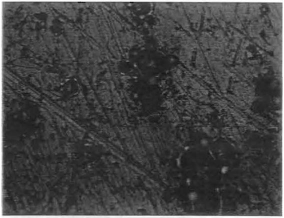

Figure 6.32. Photograph of anode surface after three 75 kV Marx bank shots -- unpolished side. Note the undamaged scratches. (X500)

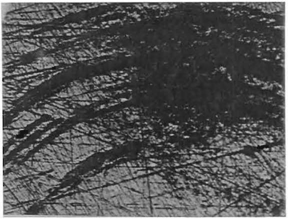

Figure 6.33. Photograph of anode surface after three 75 kV Marx bank shots -- unpolished side. Note the rings and the cluster covering a limited area. (X50)

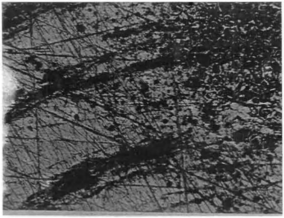

Figure 6.34. Photograph of anode surface after three 75 kV Marx bank shots -- unpolished side. Detail of the above ring of Figure 6.33. (X500)

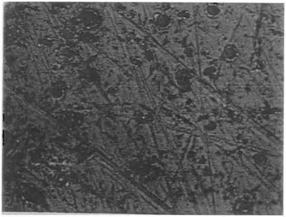

Figure 6.35. Photograph of anode surface after three 75 kV Marx bank shots -- unpolished side. Note the non-uniformity of the damage. (X500)

Figure 6.36. Photograph of anode surface after three 75 kV Marx bank shots -- unpolished side. Note the almost undamaged surface lower half of the photo. (X500)

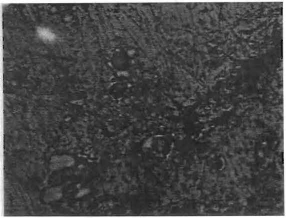

Figure 6.37. Photograph of anode surface after three 75 kV Marx bank shots -- unpolished side. Note that craters occur around the ring but not primarily on the ring. (X 500)

E. COMPARISON BETWEEN ONE AND TWO 75 KV MARX BANK SHOTS

During this stage of the work the damage on specific regions of the anode surface after one and two 75 kV Marx shots is compared. The anode on which a 75 kV Marx shot had been fired is used, and specific regions of the anode surface are compared. The same anode is subjected to another 75 kV Marx shot, and the photos are compared. The comparison of the results is of great importance, because it will demonstrate whether additional damage occurs after the second shot in the regions where damage appeared during the first shot. New photos of clusters and "chains" of craters that appeared after the second shot are also taken.

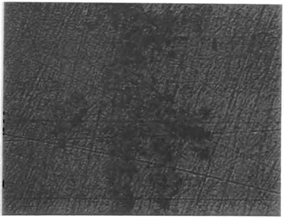

Figure 6.38. Photo of the anode surface before the second shot of 75 kV Marx bank shot. (X50)

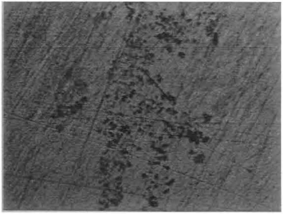

Figure 6.39. Photograph of anode surface after second shot of 75 kV Marx bank shot . Note that the same cluster seen in Figure 6.38 remains unchanged. (X50)

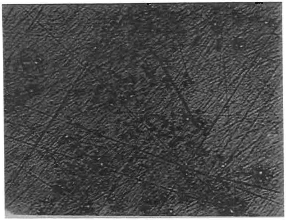

Figure 6.40. Photograph of anode surface before second shot of 75 kV Marx bank shot. This is a detail of the cluster seen in Figure 6.38. (X100)

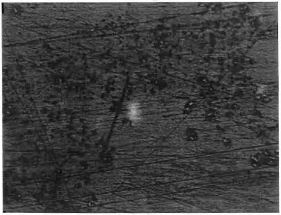

Figure 6.41. Photograph of anode surface after second shot of 75 kV Marx bank shot. Note the same scratch seen in Figure 6.40. It appears that there is no additional damage. (X100)

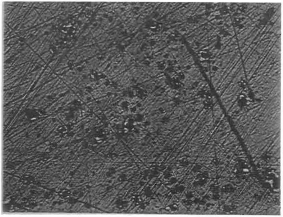

Figure 6.42. Photograph of anode surface before second shot of 75 kV Marx bank shot. Note the scratch. (X200)

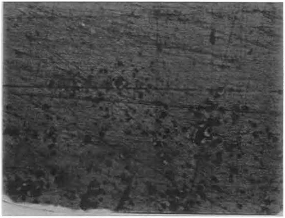

Figure 6.43. Photograph of anode surface after second shot of 75 kV Marx bank shot. Note the above section of the scratch seen in Figure 6.42. (X200)

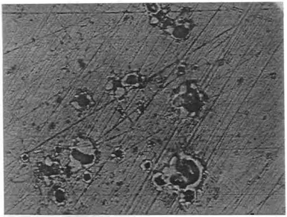

Figure 6.44. Photograph of anode surface before second shot of 75 kV Marx bank shot. (X500)

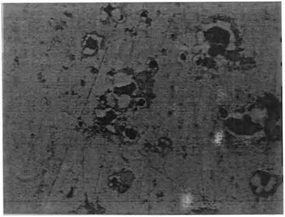

Figure 6.45. Photograph of anode surface after second shot of 75 kV Marx bank shot. Note that the region is the same as that seen in Figure 6.44. No more damage appears, except some shadowing around some of the craters. (X500)

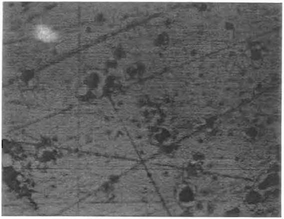

Figure 6.46. Photograph of anode surface before second shot of 75 kV Marx bank shot. Note the star of scratches (X500)

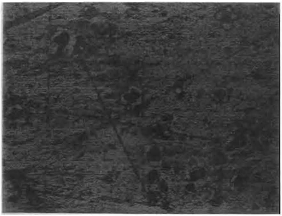

Figure 6.47. Photograph of anode surface after second shot of 75 kV Marx bank shot. Note the star (mid-photo) seen in Figure 6.45. No additional damage has occurred. (X50)

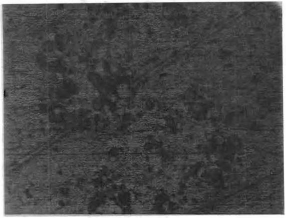

Figure 6.48. Photograph of anode surface before the second shot of 75 kV Marx bank shot. Note the crater on the scratch. (X50)

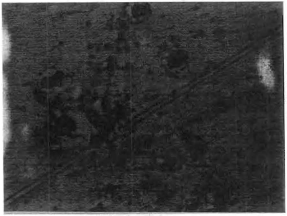

Figure 6.49. Photograph of anode surface after the second shot of 75 kV Marx bank shot. Note the same crater seen in Figure 6.47. (X50)

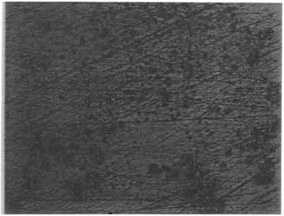

Figure 6.50. Photograph of anode surface before the second shot of 75 kV Marx bank shot. Note the scratch. (X200)

Figure 6.51. Photograph of anode surface after the second shot of 75 kV Marx bank shot. Note the same scratch seen in Figure 6.49. (X200)

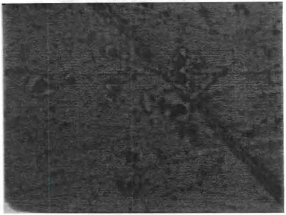

Figure 6.52. Photograph of anode surface before the second shot of 75 kV Marx bank shot. Note the craters on the scratch. (X500)

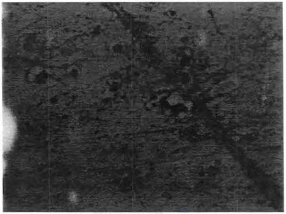

Figure 6.53. Photograph of anode surface after the second shot of 75 kV Marx bank shot. Note the same scratch seen in Figure 6.51. No more damage has occurred. (X500)

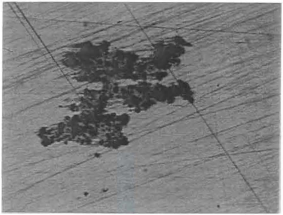

Figure 6.54. Photograph of anode surface after the second shot of 75 kV Marx bank shot. Note the new cluster. (X50)

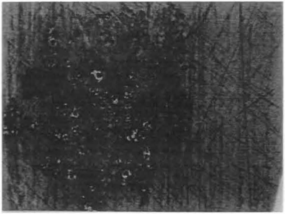

Figure 6.55. Photograph of anode surface after the second shot of 75 kV Marx bank shot. Note the new cluster. (X50)

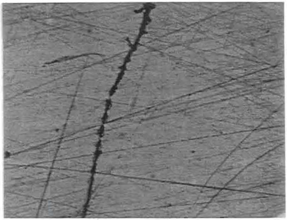

Figure 6.56. Photograph of anode surface after the second shot of 75 kV Marx bank shot. Note the chain of craters. (X50)

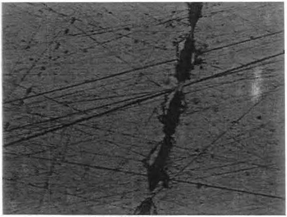

Figure 6.57. Photograph of anode surface after the second shot of 75 kV Marx bank shot. Note the chain seen in Figure 6.55. (X200)

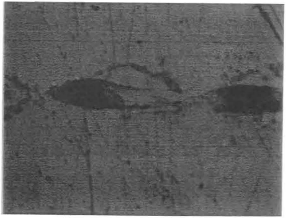

Figure 6.58. Photograph of anode surface after the second shot of 75 kV Marx bank shot. Note the chain craters. (X500)

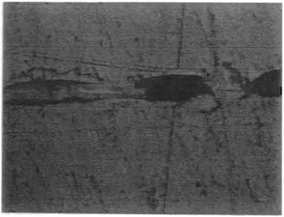

Figure 6.59. Photograph of anode surface after the second shot of 75 kV Marx bank shot. Note the chain craters. (X500)

VII. ANALYSIS

A. OVERVIEW

The experimental results of the work show extensive damage, in clusters, in limited areas on the surface of the anode electrode. As mentioned earlier, in the chapters on theory, the damage is the result of many complex events. However, the present observations enable a better understand the mechanisms, the order of the events, and the model that was applied to interpret the experimental vacuum diode; especially the anodic electrode region.

According to the Desorbed Neutral Ionization model, after the voltage onset on the diode, field emission from the cathode electrode takes place and plasma is produced in front of both the cathode and anode regions. The plasma on the anode is produced particularly due to the desorbed neutral dense layers that are just in front of the anode surface. The observations show that on some of the preexisting scratches on the surface of the anode, the craters produced and the damage sustained was significant. According to the DNI model, the desorbed neutral layer can be more dense above these scratches. This means that the damage expected on the region of scratches is large, and the craters are numerous, which shows that the observations made in this study are primarily in agreement with the DNI model (with the reservation that not all scratches have spots). The observations also include phenomena like the formation of series of craters, which go beyond the DNI model. Study of such phenomena could become significant in the expansion of the model.

B. PLASMA FORMATION ON THE ANODE SURFACE

1. Anode Surface Damage

The results of the work clearly indicate that there was considerable damage observed on all anodes of the various electrode set-ups. After two consecutive 75 kV Marx shots (equivalent to 1.04 MV inside the vacuum diode) numerous craters were observed on various points, especially near the edges of the anode electrode surface. As seen in Figures 6.1 to 6.3, some cratering was observed on preexisting scratches. This could be explained by the Desorption Neutral Ionization model, which supports the idea that the neutral dense layer (which plays a key role to the plasma production) is more dense near the edge or above scratches on the anode electrode surface. A scratched region of the anode surface is more contaminated with adsorbates like O_2 and CO_2 than the other, unscratched, well-polished surface. These adsorbate molecules are weakly bound to the surface by Van Der Waals attractions of nearly 0.25 eV, and are therefore capable of being released by the anode surface if they are given enough kinetic energy. The mechanism of release for these adsorbate molecules could be a combination of the electrical field, the impact of electrons, and ion emission. As the neutral cloud expands in front of the anode surface, it can provide a ready source for ions and secondary electrons. These secondary electrons are produced by any of the ionizing processes. These electrons are much less energetic than the high energy flux electrons, so they are a very efficient source for ionization of nearby neutrals in the cloud. The secondary electrons will ionize the surface neutrals, thus producing ions. The produced ions are then pulled toward the cathode surface.

2. Formation Of Anode Spots By Unipolar Arcing

The localized build up of plasma above the anode surface naturally leads to pressure and electrical field distributions which ignite unipolar arcing. In Figure 7.1 a picture of an anode crater is magnified 1000 times. It is believed that this crater was produced due to unipolar arcing. The center of the crater defines the "cathode" of the arc, from which electrons are emitted due to unipolar arcing process. The outer crater rim defines the electron return current area or the "anode" of the arc. The arc is called unipolar because both arc "electrodes" are located on the same metal surface. Unipolar arcing represents a discharge that easily causes explosive plasma formation. The current density, and hence the power dissipation for an arc, are considerably higher than those of field emitted or space charge limited current. The craters are formed as a result of electrical micro arcs burning between the dense plasma and the surface. So, without any external voltage applied, the arcs are driven by sheath electrical fields and plasma pressure gradients.

C. MULTIPLE ANODE SPOT CRATERS

As mentioned earlier in the analysis, extensive damage, consisting of numerous spot craters, was observed during the course of the experimental work. These craters were usually of a diameter of 10 to 20 μm, with no specific relation between size and position. Specifically, after one shot in the vacuum diode with 1.04 MV applied over the 2.5 cm gap, there were areas with clusters of anode spot craters that were surrounded by areas with no craters at all. One of these (magnified 50 times) can be seen in Figure 7.2.

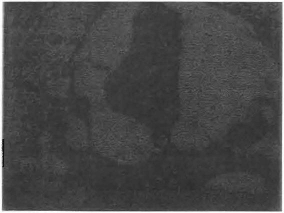

Figure 7.1. Crater produced by unipolar arcing magnified 1000 times.

This cluster consists of one main body and several "legs" of crater spots. Around this cluster there is no damage at all. Between the legs, it can be seen that there is also no damage at all. The size of this cluster is about 1.2 mm in length and 0.5 mm in width, with legs about 0.4 to 0.5 mm in length. They are visible to the naked eye, like most of the other clusters. The white lines in Figure 7.2 are scratches that resulted from smoothing and polishing the surface of the anode. It is believed that the clusters observed were in regions with many scratches as seen in Figures 6.7 and 6.24. This means that there were more dense neutral layers that, according to the Desorption Neutral Ionization model, could result in dense plasma formation, and so into many spot craters on the anode surface. The legs of the clusters had a light curve that moved in the same direction for every cluster. Even though the damage of the anode surface is mostly non-uniform at the cluster regions, almost all of the clusters had a similar shape consisting of 5 to 6 legs. For each separate cluster every leg was shifting toward the same direction (either to the right or to the left). This gives the sense of a propeller-like schematic on the stainless steel surface. The initial production of ions on the surface of the anode is highly uneven. The radial pressure gradient in the jet may contribute to the transverse motion of the ions and thus influence the divergence of an accelerated ion beam. The creation and direction of the cluster legs could be caused by magnetic forces developed during the breakdown in the anode environment. A very important part of the experimental work was the observation of the anode electrode surface after three consecutive shots of 1.04 MV in the vacuum diode chamber. This anode surface was smoothed and polished only in one-half part (semicircle) of it. There were clusters on both the polished and unpolished sides. In the unpolished region the number of clusters was slightly higher and there was significant damage on the anode surface. However, on the polished side, the size of the clusters observed were two to three times larger than the ones on the unpolished side. There were also regions between clusters with the anode surface undisturbed by the significant damage occurring in nearby regions. In Figure 7.2 a large cluster emerges in the middle of an undamaged region of the surface.

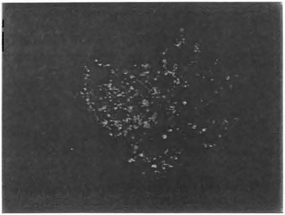

Figure 7.2. One large cluster in the middle of undisturbed surface. Note the leftward moving legs. (50X)

D. CLUSTER FORMATION

One of the most significant findings of the experiments was the formation of clusters of anode craters occurring in unpredicted areas of the anode surface. The schemes of the clusters were also different. The formation of the clusters could be caused by electron beam filaments from the cathode surface. These electron beams, under the influence of magnetic forces developed during the breakdown process, could lead to the creation of clusters of craters with legs turning to a specific direction for each cluster. It could also be affected by plasma radiation on the anode surface from several unipolar arcings, which could lead to further desorption in the same area of the anode surface.

E. POSITIONING OF THE SPOT CRATERS ON THE ANODE SURFACE

As seen in the experimental data, there is considerable damage on the anodic electrode surface. There were many groups of spot craters that formed clusters, while large portions of the anode surface remained free of spot cratering damage. This localized plasma production and hence ion emission from the anode might influence the divergence of an accelerated ion beam due to the radial pressure gradient and the magnetic field associated with the unipolar arc current. Nevertheless, it would be of great significance if the reasons why damage has occurred can be understood. The anode and cathode electrodes were marked adequately, in order to provide sufficient information about the relationship between the damage occurring on the cathode and on the anode. The results indicate that there is insufficient evidence for correlation between the place were spots occur on the cathode and on the anode. The spots are of similar size and scheme, but the places where they emerge seem unrelated, and their distribution rather non-uniform. This seems to exclude the possibility that electron beams from the cathode surface produce clusters on the anode surface. In Figure 7.3, the distribution of the spot crater groups (clusters) on the anode surface after two shots of 1.04 MV in the vacuum diode can be seen. Most of the large clusters appear in a region less than half the radius from the center of the anode, while some smaller ones appear near the edges of the anode surface. On the cathode of the same experimental set up, which is illustrated in Figure 7.4, there was no considerable damage in this region, except for some minor damage on the edge.

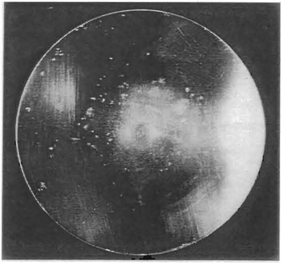

Figure 7.3. Photo showing the geometrical distribution of the clusters on the anode surface after two 1.04 MV shots. On the left side of the photo some of the clusters can be seen. The brightness on the right side of the photo is due to light reflections caused by the photo process.

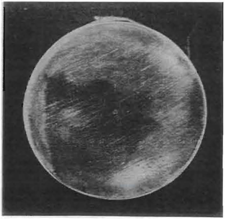

Figure 7.4. Photo of the cathode surface after two 1 MV shots. The brightness on the sides of the photo is due to light reflections caused by the photo process.

In Figures 7.5 and 7.6 the surfaces of the anode and cathode electrodes after three consecutive shots of 1.04 MV can be seen. The anode was smoothed and polished only in one half part (one semi-circle). According to observation, there was considerable damage on both parts, polished and unpolished. However, the damage on the unpolished side in some areas near the center of the electrode was deeper, and could be felt by a finger. Most of the usual clusters were found on the polished side. Nevertheless, on the unpolished side, the damage did not have the usual main body/legs (cluster) form, consisting instead of clusters of non-uniform shape. The cathode had some damage, but not clusters, and the damage that was present was generally lighter than the anode damage. The color of the cathode surface had changed to light blue, probably because of the ionization that had taken place and the thin film deposition.

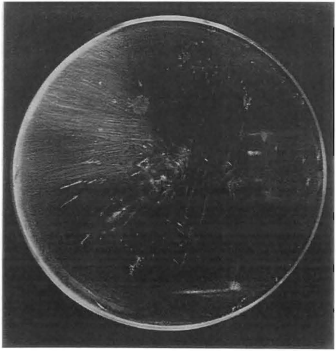

Figure 7.5. Photo of geometric distribution of clusters on the anode surface after three consecutive shots of 1.04 MV. The right side of the photograph was the polished side, and the left the unpolished side. The brightness on the upper left side is due to light reflections.

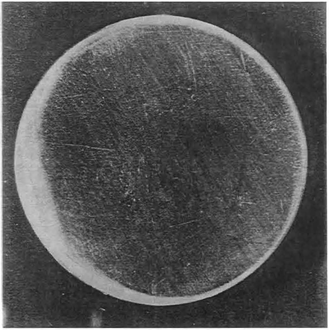

Figure 7.6. Photo showing the cathode surface after three consecutive shots of 1.04 MV. The bright sides are due to light reflections.

F. SEQUENCE OF SPOT CRATER PRODUCTION

The formation of the spot craters on the anode surface can't be sufficiently explained by the Explosive Electron Emission model (EEE), because there is not an adequate explanation of how a field emission current can be emitted from the positively charged anode surface. However, the DNI model gives a sufficient sequence of events to explain the observed phenomena.

For the vacuum diode, the onset of breakdown is typically delayed by 1 to 10 ns. This time corresponds to the time required by the desorbed neutrals to expand until they reach the maximum of the ionizing zone, where the field emitted electrons have about

100 eV. Ions produced there are accelerated back towards the electron emitting spot. The ions hit the spot with about 100 eV and recombine. This localized energy deposition leads to the surface heating and further release of adsorbed gases. The space charge of the slow moving ions will increase the electrical field, and so the field emission current, which will enhance the ionization rate. As the positive space charge increases, a double layer forms between the ions moving from the ionization zone to the cathode and the electrons moving to the anode. This reduces the applied electrical field in the gap until the electron flow becomes space charge limited. About 10 to 12 ns after the voltage onset there is plasma formation in front of the cathode surface. As the plasma density above the emitting spot increases, so does surface heating of the spot by ion bombardment. The initial plasma formation on the cathode surface of the vacuum diode is highly non-uniform. Small cathode spots of diameter 5-15 μm are formed 10-15 ns after onset of voltage due to unipolar arcing. After a short delay of 0-2 ns, a plasma layer is also formed on the anode surface. The ionization of the neutral gas layers there is caused primarily by secondary low energy electrons. With the increase of ionization rate, the potential of the ion layer increases above the anode potential, trapping the low energy electrons and forming the dense plasma layer. The sheath electrical field causes small microsized unipolar arcs to form on the anode surface, which results in the anode crater spots.

G. COMPARISON BETWEEN 1 AND 2 SHOTS OF 1 MV DIODE VOLTAGE

To better understand the physical processes that govern the plasma formation process on the anode surface an attempt was made to specify the differences between observed parts of the same anode after one and two shots of 1.04 MV inside the vacuum diode of the FXR facility. As can be seen in Figures 6.25 - 6.32, the clusters that were observed before and after the second shot were unchanged regarding to their shape and the number of spot craters. At the same time, other clusters were observed in various other places with a distribution which is considered as non-uniform. On the anode surface, as can be seen in Figures 6.55 and 6.58, after the second shot of 1.04 MV some curved lines of spot craters where present that did not exist after the first shot. This might have to do with the magnetic forces appearing in the plasma environment. Another impressive observation came after the comparison between the same region of the stainless steel anode surface after one and two shots, magnified 500 times, as can be seen in Figure 5.32. There it appers that after the second shot, around the preexisted crater spots appeared to form a shadowing region which could represent layers of neutrals which were not sufficiently ionized in order to initiate the process for plasma formation. Nevertheless as can be seen after the comparison of Figures 6.38 through 6.52 the damage sustained on the regions that were observed was not enhanced from the existence of previous craters. Apparently in anode regions observed before and after the second 1.04 MV shot, there were no more damage that could be associated with the presence of the previous craters.

This could be explained by the insufficient dense neutral layers, above the tiny previous craters, to produce new unipolar arc burnings. After the first shot the surface is relatively clean due to "discharge cleaning" in the areas where clusters have formed. Hence, after the second shot no further damage is caused due to less desorption. It could also be explained by the behavior of the electron beams - filaments from the cathode which hit other areas of the anode.

VIII. CONCLUSIONS AND RECOMMENDATIONS

The purpose of the completed work was to determine whether spot craters and thus, plasma formation occur in the region in front of the anode surface of the diode of a high voltage pulse powered system. It was also the purpose of this study to investigate the geometrical characteristics of the spot craters which are formed on the anode surface and whether anode damage is affected by scratches and other abnormalities on the anode electrode surface. The results of the experimental work indicate that anode craters really exist and plasma formation takes place in front of the anode surface. However, the comparison between one shot and two shot photos showed that previous damage spots on the anode surface caused by the first shot do not induce larger damage spots after the second shot. The creation of new crater spots indicates that new anode damage is independent of old damage, and thus does not depend on previous crater formation. On the other hand, the photographs show that in certain locations spot craters are formed in a line on a preexisting scratch, but not all scratches have anode spot craters on them. This means that the critical conditions for onset of unipolar arcs depend on several parameters: surface roughness, adsorbed impurity layers, energy deposition by energetic primary electrons and ionization rates by lower energetic secondary electrons. Another impressive finding was the formation of clusters of craters which were found on the anode surface. They consist of many craters and are surrounded by undamaged surface area. They have "legs" which for each cluster turn in the same direction. This indicates that magnetic fields could play a key role to the investigated phenomena. Another new observation was that some curved lines were observed after the second shot. These lines consist of craters different from the normally circular craters. The formation of these series of craters may support the idea that magnetic fields affect significantly the phenomena observed on the anode surface. The marking of the anode and cathode electrodes showed that there is no direct relation between damage which occurred on the cathode and anode surface. It was also indicated that the formation of craters on the anode surface was non-uniform and unpredictable. However most of the cluster areas were formed in the region around the center of the anode electrode surface. This may be due to electron beams emitted from the edge area of the cathode, or pinching. The Desorbed Neutral Ionization model (DNI) explains the formation of craters above preexisting scratches. Furthermore, the DNI model helps to understand why in regions with preexisting damage, after a new shot there is no new damage recorded. The cratered surface has been discharge cleaned by the first shot. The reduction of adsorbed neutrals inhibits the formation of unipolar arcs. The DNI model may need to be expanded in order to include an explanation of the magnetic field behavior during the break down process in a high pulse powered system. Further work in this area is needed in order to better understand the mechanisms which cause the plasma formation on the anode surface. A theoretical study of the development of the magnetic fields would help us to understand the distribution of craters formed on the anode surface. More work could also be done to investigate the geometrical distribution of the damage on the electrode surface. More materials like Al, Zn, Cooper could be used in order to provide comparable results with stainless steel. Further investigation should also be made of the role that is played by the preexisting scratches and especially by their depth. Generally, this work showed that the

DNI model needs to be expanded in order to include magnetic force effects and to study preexisting scratch effects. New materials could be used in order to provide expandable data for the plasma formation on the anode surface. This could be very significant for understanding the mechanisms which occur in the diode of a high voltage system.

APPENDIX. OPERATIONAL PROCEDURES OF PULSERAD 112A

A. PREPARATION OF PULSERAD 112A FOR OPERATION

The operating instructions of the Pulserad system are given in detail in [Ref. 23]. Here, the procedure is summarized.

1. Set of the Cathode-Anode spacing in the Accelerating Tube

The cathode-anode spacing is set to 2.54 cm, and the cathode adjustment is made using the following procedure:

1. Remove the anode plate assembly and the O-ring from the front flange.
2. Loosen set screw on the cathode support stem and place straight edge across front flange.
3. Measure from edge of straight edge facing the cathode to the cathode tip surface. In order to take the actual cathode surface spacing, add 6.35 cm to this measurement. So, in this case, in order to obtain a cathode -anode spacing of 2.54 cm the cathode is set to measure 19.05 cm.
4. Tighten set screw on cathode support stem and recheck measurement.

For the installation of the anode electrode, the following procedure is used:

1. Lay the anode face plate on the flat non marring surface with diode side facing down and cut a disc to fit into anode machined recess.
2. Install a cleaned O-ring into groove on face plate and fasten the anode cover plate.
3. Install a cleaned greased O-ring in the machine's front flange and position and fasten the anode plate assembly onto the front flange.

2. Start the Vacuum System

The Pulserad 112A system is ready to be operated when the pressure in the accelerator tube is lower than or equal to 5×10^{-4}Torr.

3. Marx Generator

The desired voltage for the experiment is 75 kV. So, the Blumlein pulse charge voltage is given in [Ref. 21] by the relation:

Bl. Volt. = 12 x1. 2 x . 9 x Marx Voltage

For present purposes, Marx voltage is 75 kV, so

Bl. Volt. = 12 x 1. 2 x. 9 x 75 = 972 kV

The diode voltage is given by:

Diode Volt. = 2 x Bl. Volt. x 50 /93 = 1. 04 MV

The factor 50/93 expresses the impedance of the system circuits.

4. Charging and Firing the Pulserad 112A

In order to achieve a successful functioning of the Pulserad system the following procedure should be followed:

1. Observe all the safety precautions and ensure that all personnel are cleared from the Pulserad area.
2. Set all switch pressures at the proper values and adjust the dc kilovolt meter set point to the desired Marx charge voltage.
3. Turn on the Pulsepak 10A power and high voltage and turn the power supply key to the run position.
4. Press the 'HV start' button and when the dc kilovolt meter reaches the pre-selected setting, the system is ready to fire. This is done by depressing the fire button on the Pulsepak 10A device.
5. Turn off the Pulserad power supply key removing it from console and turn off the trigger system power.

LIST OF REFERENCES

1. Mesyats, G.A., and Proskurosky, D.I., *Pulsed Electrical Discharge in Vacuum*,v. 5, Springer-Verlag, 1989.

2. Schwirzke, F., "Formation of Cathode Spots by Unipolar Arcing," *Gaseous Dielectrics VI*, Ed. L. G. Christophorou and I. Sauers, p. 209 - 214, Plenum Press, New York, 1991.

3. Wright , C., "Time Resolved Measurements of Light Produced by Onset of Plasma Formation on Electrodes of Fast Pulsed High Voltage Diodes," Master's Thesis, Naval Postgraduate School, Monterey, California, December 1993.

4. Miller, R.B., "An Introduction to the Physics of Intense Charged Particle Beams," Plenum Press, New York, 1982.

5. Parker, R., "Explosive Electron Emission and the Characteristics of High Current Flow," Air Force Weapons Laboratory, Kirtland Air Force Base, N.P., 1974.

6. Hallal, M.P.,Jr., "The Onset of Breakdown in a fast Pulsed Vacuum Diode," Master's Thesis, Naval Postgraduate School, Monterey, California, June 1992.

7. Callahan, M., "X ray Pulse Considerations and Electron Flow in High Voltage Diodes," Master's Thesis, Naval Postgraduate School, Monterey, California, December 1993.

8. Kittel, C. and Kroemer H., *Thermal Physics, 2nd ed.*, W. H. Freeman and Company, New York, 1980.

9. Barnett, C.F. Ray J.A., and Thompson J.C., *Atomic and Molecular Collision Cross Sections of Interest in Controlled Thermonuclear Research*, p. 141, Oakridge National Laboratory, 1964.

10. Schwirzke, F., Maruyama X.K., Hallal, M. P. Jr., "Ion Formation on the Surfaces of Electrodes," *Nuclear Instruments and Methods in Physics Research*, Section B, Elsevier Science Publishers B.V., 1992.

11. Willis, G., "Investigation of Onset of Plasma Formation at Anode of Fast Pulsed High Voltage Vacuum Diode," Master's Thesis, Naval Postgraduate School, Monterey, California, March 1993.

12. Miller, C., "Vacuum Arc Anode Phenomena," *IEEE Transactions on Plasma Science* Vol. ps-11, No 2, pp. 76 - 89, June 1983.

13. Miller, C., "Discharge Modes at theAnode of a Vacuum Arc," *IEEE Transactions on Plasma Science*, Vol. PS 11, No 3, September 1983.

14. Kimblin, C.W., "Ion Currents Associated with the Anode spots of Vacuum Arcs," *Xiii Nt. Conf. Phen. Ion. Gases*, p. 243, Eindhoven, 1975.

15. Kimblin C.W., "Erosion and Ionization in the Cathode Spot Regions of Vacuum Arcs," *J. Appl. Physics*, Vol. 44, p 3704 - 3081, 1973.

16. Bacon F.M., "Vacuum Arc Anode Plasma Spectroscopic Investigation," *J. Appl. Physics*, Vol 46, p 4750 - 4757, 1975.

17. Yokohama, T. and Kashitani, Y., "An Observation Ofarcing Under Vacuum," *Meiden Rev.*, Vol 56, no. 2, p 60 -64, 1979.

18. Frind G., Caroll J., Goody, P., and Tuohy E.J. "Recovery Times of Vacuum Interrupters Which Have Stationary Anode Spots," *IEEE Trans. Power Syst.*, Vol. PAS -101, p775 - 784, 1982.

19. Zycova, N. M., and others, "Cathode And Anode Regions In An Electric Arc : I. Cathode And Anode Regions At Low Pressures And In Vacuum," *Sov. Phys. Vol 15*, pp 1844 - 1849, 1970.

20. Grissom J.T., and Newton, J.C., "Anode Surface Radiance from Microsecond Vacuum Arcs," *J. Appl. Physics*, Vol. 45, pp. 2285-2294, 1974.

21. Rich J. , Prescott L.E. and Cobine J.D., "Anode Phenomena in Metal Vapor Arcs at High Currents," *J. Appl. Physics*, Vol. 42, p587 - 601, 1971.

22. Goldsmith S., and Boxman R. L., "Excited State Densities in a Multicathode Spot AL Vacuum Arc, II. Theoretical Approach," *J. Appl. Physics*, Vol. 51, p 3649 - 3656, 1980.

23. Goldsmith S., Shale F. S., and Boxman R. L., "Anode Melting in a Multicathode Spot Vacuum Arc," *IEEE Transactions on Plasma Science*, Vol. PS 11, No 3, p 127 - 132, September 1983.

24. Physics International Company , *Model 112a Pulserad Pulsed X-Ray Generator Operations and Maintenance Manual*, January, 1986.

25. Physics International Company , *Model 112b Pulserad Pulsed X-Ray Generator Operations and Maintenance Manual*, February, 1987.

26. Carl Zeiss, *Operating Instructions Manual for Model ICM405*, October 1978.

INITIAL DISTRIBUTION LIST

1.	Defense Technical Information Center Cameron Station Alexandria, VA 22304 - 6145	2
2.	Library, Code 52 Naval Postgraduate School Monterey CA 93943 - 5101	2
3.	Professor Fred Schwirzke, Code PH/Sw Department of Physics Naval Postgraduate School Monterey CA 93943 - 5117	2
4.	Professor Xavier K. Maruyama, Code PH/Mx Department of Physics Naval Postgraduate School Monterey CA 93943 - 5117	2
5.	Professor R.W. Ashton, Code EC/Ah Department of Electrical and Computer Engineering Naval Postgraduate School Monterey, CA 93943 - 5121	2
6.	Professor William Colson, Code PH/Cw Chairman, Department of Physics Naval Postgraduate School Monterey, CA 93943 - 5117	1
7.	Chairman, Code EC Department of Electrical and Computer Engineering Naval Postgraduate School Monterey, CA 93943 - 5121	1
8.	Lt Vassilios Stamatopoulos 30 Nikitara Str. Pirueus 18544 Athens Greece	2

DUDLEY KNOX LIBRARY
NAVAL POSTGRADUATE SCHOOL
MONTEREY CA 93943-5101

GAYLORD S

DUDLEY KNOX LIBRARY
3 2768 00305886 8